Journal of the Geological Society, London, Vol. **164**, 2007, pp. 795–814. Printed in Great Britain.

Cenozoic behind-arc volcanism in the Bolivian Andes, South America: implications for mantle melt generation and lithospheric structure

LEONORE HOKE* & SIMON LAMB

Department of Earth Sciences, Parks Road, Oxford OX1 3PR, UK (e-mail: simon.lamb@earth.ox.ac.uk)

**Present address: 14 Oriental Street, Lower Hutt, New Zealand*

Abstract: We develop a model of arc and behind-arc volcanism, as well as constraining the evolution of the lithospheric mantle structure beneath the Bolivian Andes during the last 25 Ma, using new geochronological and geochemical data on behind-arc mafic volcanic rocks, together with a regional isotopic study of geothermal helium emissions, and a comparison with seismic tomographic images of the same region. Helium isotopes measured in natural gas emissions in geothermal and mineral-water springs suggest recent mantle melting in a wide zone extending at *c*. 20°S from a few tens of kilometres west of the volcanic arc to over 300 km behind the arc, where the subducted slab is at depths increasing from *c*. 100 to *c*. 250 km. During the Neogene, there has been behind-arc mafic–felsic magmatism right across the high Andes between 17° and 22°S, in the Altiplano and western margin of the Eastern Cordillera. Modelling of Plio-Pleistocene basalts and basaltic andesites (<5.2 Ma), using REE, suggests that the main melt source region is in spinel and spinel–garnet peridotite, at depths <100 km. In detail, the best-fit REE inversions suggest two spatially distinct melt zones: (1) a *c*. 15% depleted mid-ocean ridge basalt (MORB) source at depths between *c*. 75 km and *c*. 110 km for mafic volcanic rocks that crop out <75 km behind the arc; (2) a slightly enriched MORB source at depths between *c*. 65 km and *c*. 90 km for those that crop out >100 km behind the arc. REE inversions for Oligo-Miocene shoshonites and basalts (*c*. 25–21 Ma) suggest that they originated at significantly shallower depths (*c*. 45 km to *c*. 100 km) from a slightly enriched MORB source. Eruption of shoshonitic lavas also occurred in the Altiplano between 13 and 11 Ma, and widespread behind-arc intermediate–felsic volcanism has been more or less continuous since the early Miocene. All this suggests that since *c*. 25 Ma there has been a thin (<100 km) lithosphere beneath the high part of the Bolivian Andes. Long-lived mantle melting is best explained by wet adiabatic decompression in the upwelling part of the corner flow in the mantle wedge, controlled by the lithospheric thickness variations, with depleted melt advected into the melt zone beneath the arc. Widespread arc and behind-arc magmatism may have been triggered at *c*. 25 Ma by the opening up of a mantle wedge and inflow of hot asthenosphere, as a consequence of the steepening of the subducted slab and detachment of hydrated and weakened mantle lithosphere and possibly mafic lower crust.

There is now widespread recognition that mantle processes can play an important role in the tectonics of mountain belts, and changes in the lithospheric mantle (either thickening or thinning) can have an important effect on surface uplift, volcanism and lithospheric strain (Houseman *et al*. 1981; England & Houseman 1989; Molnar *et al*. 1993; Platt & England 1994; Hoke *et al*. 2000; Garzione *et al*. 2006).

In this paper, we investigate the Cenozoic lithospheric mantle evolution beneath the high parts of the Central Andes, mainly in Bolivia, but also northern Chile and northwestern Argentina. This region forms the second highest broad region on Earth, with widespread mafic volcanism since the Late Oligocene (Davidson & de Silva 1995; Lamb & Hoke 1997). Farther south, in the Puna region of northwestern Argentina, Coira *et al*. (1993), Kay & Kay (1993) and Kay *et al*. (1994) have proposed a relationship between magmatism, mantle delamination and changes in the subduction geometry.

Seismic tomography studies of South America suggest marked variations in the lithospheric thickness (see below). Here we use an independent method, based on the geochemistry of mafic magmatic rocks and helium isotope signatures of natural gas emissions, to define the extent and depth of mantle melting beneath the Central Andes. We use this, together with an understanding of the processes of melt generation and melt extraction, to make inferences about the thermal state of the mantle throughout the Cenozoic, placing constraints on the depth of the base of the lithosphere (Turcotte & Schubert 2002).

Our work follows on from earlier studies (Hoke *et al*. 1994, 2000), which used the isotopic signature of helium as a tracer for mantle-derived volatiles in the Andes and Tibet. We present a new regional compilation of helium isotopic data for natural gas emissions in the Central Andes (this study; Hilton *et al*. 1993; Hoke *et al*. 1994), together with new geochemical and geochronological data for mafic volcanic rocks sampled across the Altiplano region. We use these data to investigate the lithospheric structure, comparing our results with existing seismological and gravity studies. We compare these constraints with existing models of melt generation in subduction zones.

We show that the main features of the lithospheric structure beneath the high Andes, with a wide zone of shallow mantle melting and relatively thin lithosphere compared with that farther east, have existed for the last *c*. 25 Ma. We suggest that lithospheric thinning was linked to the resumption of arc volcanism, after a period of quiescence in the preceding *c*. 10 Ma, triggered by steepening of the subducted slab at *c*. 25 Ma and detachment of part of the overlying lithosphere, with concomitant upwelling of relatively hot asthenospheric mantle and widespread shallow mantle melting. This view of the evolution of the Bolivian Andes is in marked contrast to some recent models that have proposed catastrophic and massive

delamination of the lithosphere beneath the Bolivian Altiplano around 10–7 Ma (Garzione *et al*. 2006).

Tectonic setting of the study area

The Central Andes are situated on the western margin of South America where the Nazca oceanic plate is being subducted beneath the continental lithosphere of the South American plate at *c*. 80 mm a^{-1} in a roughly ENE direction (Fig. 1, NUVEL-1A; DeMets *et al*. 1994). A well-defined Benioff zone dips at *c*. 30° beneath the study area, shallowing to a flat subduction farther north and south (Cahill & Isacks 1992). The finite relative plate motions are reasonably well known for the past 68 Ma (Pardo-Casas & Molnar 1987).

The study area lies at the latitudes of the Bolivian Andes (Fig. 1). Widespread diffuse shallow seismicity shows that this region is actively deforming, and the long-term evolution can be constrained from a wealth of geological data obtained from the deformed thick and extensive sedimentary basins that formed both before and during mountain building (Sempere *et al*. 1990; Allmendinger *et al*. 1997; Lamb & Hoke 1997; Lamb *et al*. 1997).

The Bolivian Andes can conveniently be divided into several physiographic and geological provinces (Fig. 1). The high central plateau of the Altiplano, which is at an average elevation of *c*. 3.8 km and up to 200 km wide, is bounded to the west by the volcanic arc (Western Cordillera) and fore-arc in northern Chile and southern Peru, and to the east by the rugged Eastern Cordillera. The Eastern Cordillera locally reaches elevations up to 6.5 km in the Cordillera Real and becomes progressively lower in the sub-Andean zone, the latter forming a thin-skinned fold and thrust belt. Earthquakes show that the eastern margin of the sub-Andean zone is the locus of active deformation, accommodating underthrusting of the foreland region comprising the Brazilian Shield (Watts *et al*. 1995; Lamb 2000).

Lithospheric and crustal thickness variations in the Central Andes

Yuan *et al*. (2002) have shown that there are departures in the relation between crustal thickness and surface elevation in the Central Andes, which are most easily explained in terms of a variable thickness of the mantle part of the lithosphere. The total thickness of the lithosphere ranges between 100 and >150 km, whereas crustal thickness varies between *c*. 37 km beneath the foreland immediately east of the Bolivian Andes, and up to

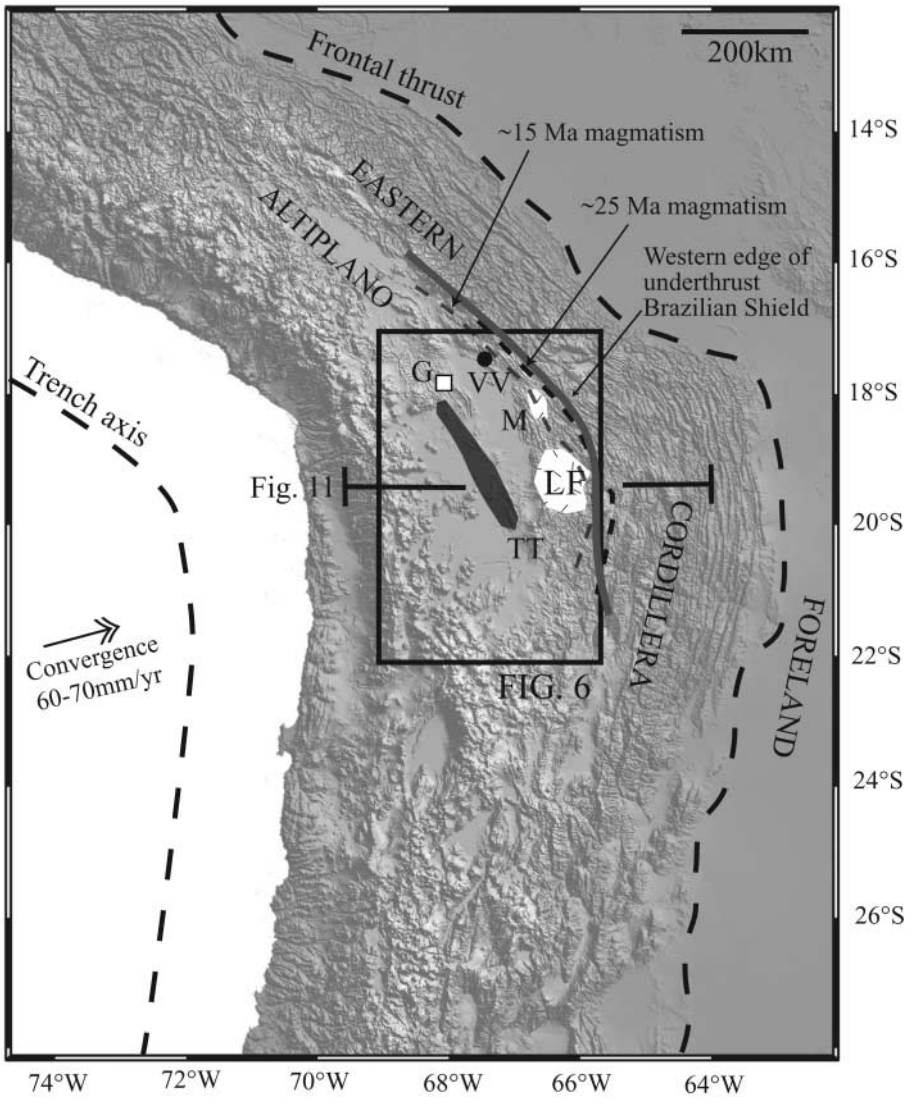

Fig. 1. Map showing the tectonic setting and topography of the Central Andes. Large box shows the location of the study area (see Fig. 5). The region can be divided into a number of physiographic provinces: the Eastern Cordillera mainly consists of Lower Palaeozoic flysch-like sequences, generally at altitudes of 3–4.5 km; the Altiplano forms a high plateau region of subdued relief at elevations of *c*. 4 km, underlain by thick Cenozoic red-bed sequences; the volcanic arc lies on the western margin of the Altiplano, referred to as the Western Cordillera, and consists of spaced andesitic cones and small dacitic domes, rising nearly 2 km above the general level of the surrounding regions. West of the volcanic arc, the Andes slope down toward the fore-arc and Pacific Ocean. Short-dashed lines show easternmost limit of *c*. 25 Ma and *c*. 15 Ma magmatism. The undeformed 12–1.5 Ma Los Frailes volcanic complex (LF) and 24–10 Ma older stocks and intrusions and 9–5 Ma Morococala ignimbrites (M) crop out on the Western margin of the Eastern Cordillera. The location of voluminous Altiplano mafic magmatism is shown in black (TT, Oligo-Miocene (25–21 Ma) behind-arc mafic lavas and intrusions; VV, 13–11 Ma Vila Vila shoshonitic lava field). White square (G) shows location of the palaeoaltimetry study by Garzione *et al*. (2006). (See Fig. 11 for cross-section.)

80 km beneath the Altiplano (Wigger *et al*. 1993; Beck *et al*. 1996; Yuan *et al*. 2002), in the regions of maximum elevation.

The thickness of the lithosphere beneath the volcanic arc must be less than the depth to the top of the subducting slab, to allow room for a convecting asthenospheric mantle that could act as a long-lived source of arc volcanism (Davies & Stevenson 1992). This constrains the lithosphere in this region to be $<$120 km thick. Heat-flow studies (Pollack & Chapman 1977; Henry & Pollack 1988; Springer 1999) suggest that the base of the lithosphere, if defined by an isotherm (Ranalli 1995) that is some fraction of the mantle melting temperature T_m (e.g. $0.85T_m$), may lie at depths of a few hundred kilometres beneath the Brazilian Shield.

There have been several attempts to image the seismic velocity structure of the mantle beneath South America for P and S waves (Whitman *et al*. 1992, 1996; Widiyantoro & van der Hilst 1997; Myers *et al*. 1998; James & Sacks 1999; Van der Hilst & Karason 1999; Fukao *et al*. 2001; Van der Lee *et al*. 2001), although, so far, the resolution of the seismic tomographic models has been poor, largely because of a non-ideal arrangement of seismic sources and receivers that prevents proper sampling of the lithosphere and underlying mantle. Regional S-wave models show (Fig. 2a–c) that the cratonic cores of South America, in the Brazilian and Guyanan Shield areas, extend to depths of 250 km and are associated with fast velocity anomalies up to +1.5% (Van der Hilst & Karason 1999). Regional high-resolution P-wave tomographic models seem to resolve more detail, showing this fast 'lid' becoming markedly thinner towards the Central Andes, where there are even negative velocity anomalies (Fig. 2b and c, Widiyantoro & van der Hilst 1997; Fukao *et al*. 2001). These features are essentially shared by the high-resolution S-wave model for South America of Van der Lee *et al*. (2001), with a broad slow zone beneath much of the Central Andes, although the fast lid beneath the Brazilian Shield is less than 150 km thick (Fig. 2a and b). This image of South America is similar to that derived from gravity studies (Fig. 2d): the cratonic cores, in the Brazilian and Guyana Shields, are associated with high flexural rigidities (elastic thickness T_e $>$75 km), and the rigidity becomes progressively less towards the Andes (Whitman *et al*. 1992; Watts *et al*. 1995; Stewart & Watts 1997; Black 2000).

Evidence for mantle melting

The most direct evidence for mantle melting and melt extraction comes from mafic magmatism. Dating this magmatic activity places constraints on the thermal history of the underlying mantle, and may also provide clues to changes through time in lithospheric structure. However, for small mantle melt fractions, there is a high probability that the melt will freeze within the crust or mantle, and never reach the surface. For this reason, the extent of surface manifestations of mafic volcanism and shallow mafic intrusions may not show the full extent of the underlying mantle melt region. A better guide may be the presence of mantle helium in natural gas emissions, because incompatible volatile phases such as helium are strongly partitioned into the

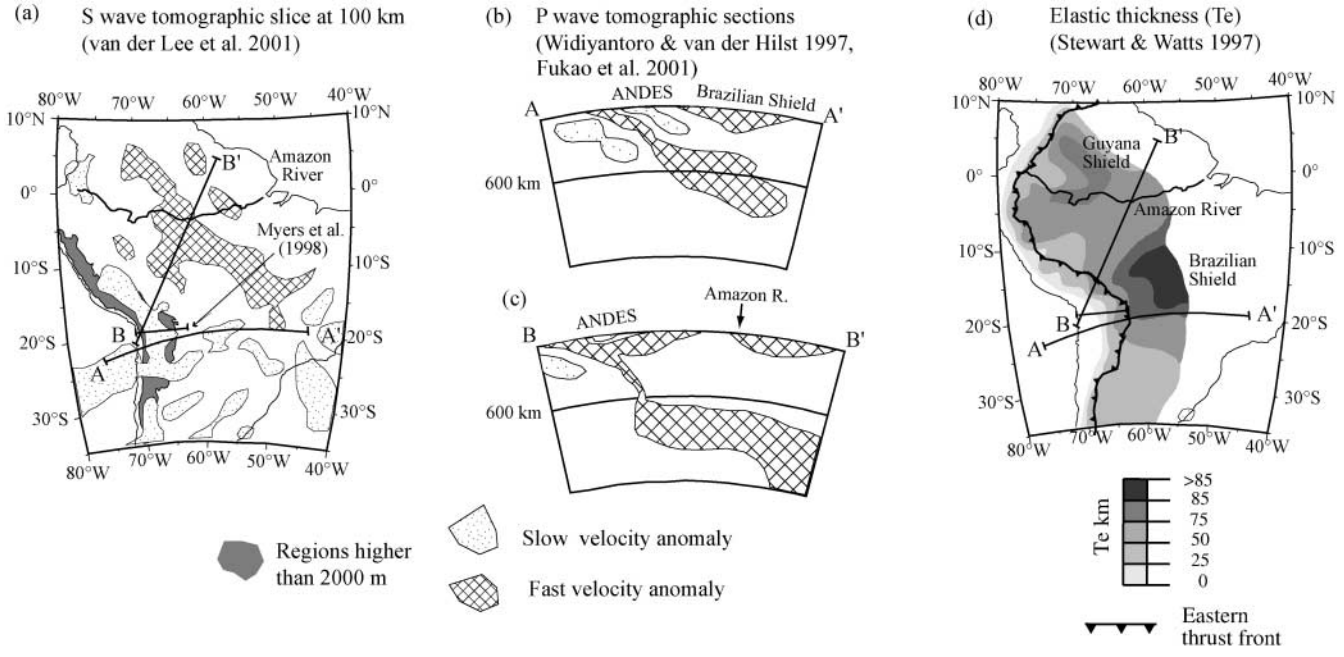

Fig. 2. Seismic tomography and T_e. (**a**) Map view of Van der Lee *et al*. (2001) S-wave model, showing a horizontal slice at 100 km. The model shows a slow zone beneath the volcanic arc, but extending farther east beneath the Altiplano (regions higher than 2000 m). In addition, high velocities are generally associated with the Guyana and Brazilian Shield areas, much farther east. However, south of the fast zone, plume-like patches of slow zones also appear in the foreland, contrary to the high-resolution P-wave model in (**b**), which shows a thick fast lid. Cross-sections AA′and BB′ are shown in (**b**) and (**c**). (**b**) Cross-section of high-resolution P-wave model along AA′ in (**a**) (Widiyantoro & van der Hilst 1997; Fukao *et al*. 2001), showing a thick (up to 250 km) fast lid beneath the foreland, east of the Andes, in the vicinity of the Brazilian Shield. The fast lid becomes progressively thinner farther west towards the Andes, which are associated with underlying slow zones. (**c**) Cross-section of high-resolution P-wave model, as in (**b**), along BB′ in (**a**), showing two fast lids associated with the Brazilian and Guyana Shields in the foreland. (Note how this model shows a relative slow zone beneath the Amazon basin, which is not resolved by the S-wave model in (**a**).) (**d**) T_e structure for South America, based on an analysis of gravity and topography (Stewart & Watts 1997). (Note how this resolves high T_e ($>$50 km) associated with the Brazilian and Guyana Shields, with T_e becoming progressively less towards the Andes.)

melt. The volatiles will rise with the melt, and, if the melt reaches the brittle crust, will eventually be advected to the surface by deeply circulating groundwater systems, even if the melt itself becomes trapped at depth. For instance, helium sampled at the mid-ocean ridges, measured in basaltic glass rinds from pillow basalts, has a relatively uniform isotopic ratio, where $^3He/^4He = 10^{-5}$ or *c*. 8 R_a, where R_a is the isotopic ratio of helium in the atmosphere. Helium emitted from deeply sourced mantle plumes, such as the Hawaiian plume, can be even more enriched in ^3He, with a $^3He/^4He$ ratio of *c*. 2.5×10^{-5} or even up to 50 R_a (Stuart *et al*. 2003). On the other hand, crustally derived helium is predominantly alpha particles, ^4He, from the decay of U and Th (with minor nucleogenic ^3He generated by neutron collision with ^6Li), and has a $^3He/^4He$ ratio of *c*. 10^{-8}, or 0.01 R_a (Ballentine & Burnard 2002). This three orders of magnitude difference in $^3He/^4He$ ratio, depending on its source, makes helium isotopes an excellent tracer of mantle-derived volatiles, released during mantle melting. Helium can be readily sampled in geothermal and mineral-water springs and also in mineral fluid inclusions (e.g. in olivine). The residence time of helium in the crust is likely to be small ($\ll$1 Ma), and so mantle helium emissions at the surface can be used as an indication of recent or active mantle melting (Hoke *et al*. 2000). A full description of helium systematics and the methods used in this study have been given by Poreda & Farley (1992), Giggenbach & Poreda (1993) and Hoke *et al*. (1994, 2000).

In this study, we map out the zones of active and Cenozoic mantle melting in the Central Andes by first describing the regional helium isotope characteristics of the Central Andes between *c*. 17 and *c*. 25°S using published (Hilton *et al*. 1993; Hoke *et al*. 1994) and new data (this study), followed by the temporal and spatial distribution of mafic volcanism and shallow intrusions and their chemical characteristics in the Altiplano back-arc region.

Helium emissions in the Central Andes

Helium isotope map

A summary of the regional distribution of helium isotopic ratios measured in natural gas emissions (geothermal and mineral-water springs, fumaroles and sulfataras) in the Central Andes is shown in Figure 3 and Table 1. Our new data (Table 1), together with those previously published (Hilton *et al*. 1993; Hoke *et al*. 1994) make it possible to contour the spatial distribution in terms of the R/R_a values (Fig. 3a). This contour map is also extrapolated into regions for which there are no data; here the contours tend to balloon out as 'edge effects'. In an attempt to minimize such

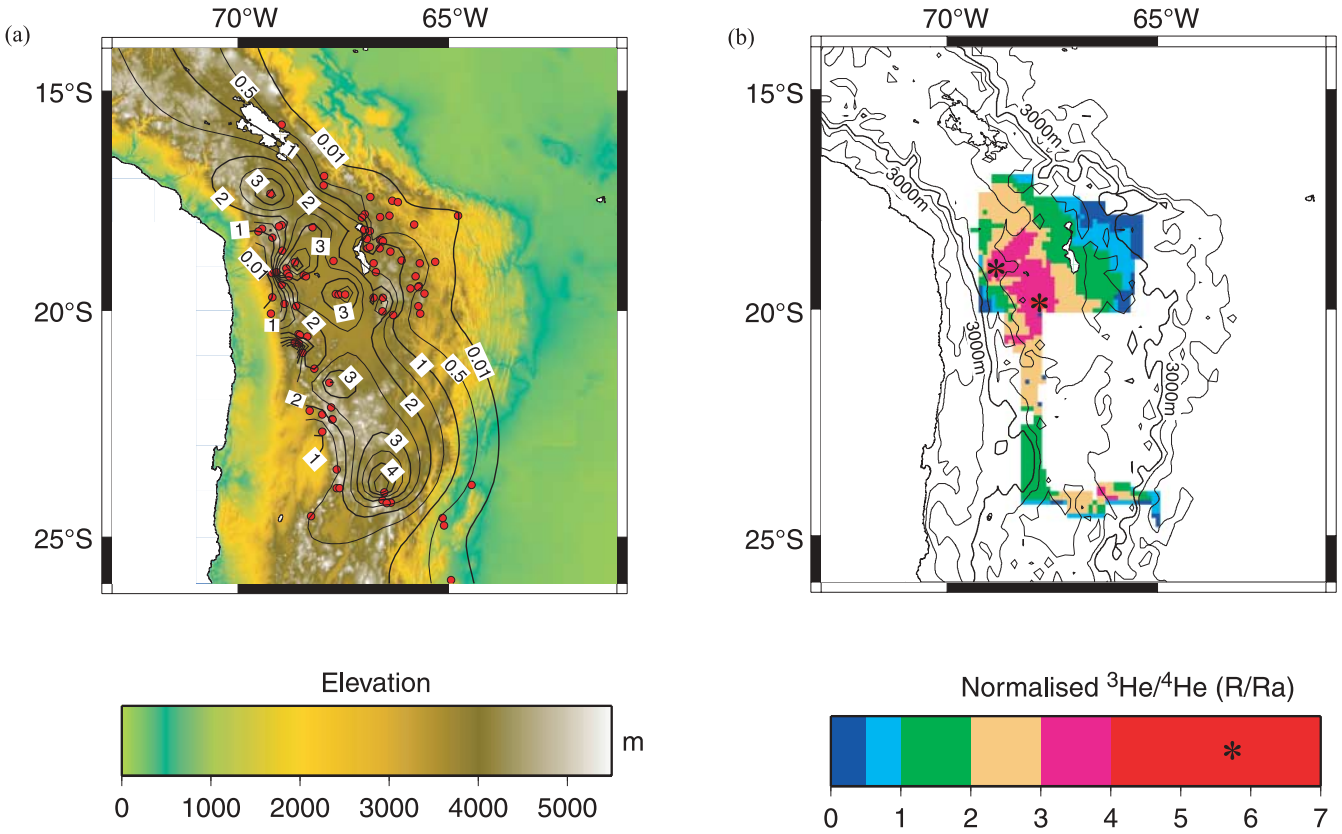

Fig. 3. Topographic map of the Central Andes between *c*. 14°S and *c*. 26°S, showing the location of natural helium emissions sampled for helium isotopic analysis (●, this study; Hilton *et al*. 1993; Hoke *et al*. 1994). The helium $^3He/^4He$ is expressed as R/R_a values (see text), ranging from $\ll$0.5 to *c*. 6. (**a**) R/R_a values contoured using a best-fit surface to the data. Contours tend to balloon out where there are no data. However, the following general features are clear: (1) contours mimic the general shape of the Central Andes, with its pronounced bend at *c*. 17°S; (2) the high values along the arc, in the west, are associated with active volcanoes, spaced *c*. 50–100 km apart; (3) high values extend much farther east, into the Altiplano and western margin of the Eastern Cordillera; there is a sharp cut-off to low values (<0.5) on the western and eastern margins of the Andes. (**b**) The same data as in (**a**), but contoured only where data points are densest, revealing essentially the same pattern as in (**a**). Asterisks mark R/R_a highs >5.

Table 1. *New helium isotope analyses in the Central Andes*

Locality	Lat., long.	Altitude (m)	Type	*T* (°C)	pH	R/R_a	X	[He]C μcm^3 STP g^{-1})	c.CO_2 (μcm^3 STP g^{-1})	R_c/R_a	%Mantle He
Volcanic arc (Western Cordillera), Bolivia and northern Chile											
Laguna Sacabaya (A)	18°39′, 68°58′	3800	s/w			1.77	3948	W		1.768	24.7
Irrutupuncu	20°43′, 68°39′	3800	s/w	56	3	2.35	2.14	0.01	0.4715	3.53	50.1
Volc. Irrutupuncu	20°44′, 68°32′	4950	ss/g	400		4.96	n.d.	–	1.1414	4.96	70.7
Volc. Irruputuncu (R)	20°44′, 68°33′	4920	fs/g	72		5.633	716	–		5.64	80.5
Volc. Irruputuncu (R)	20°44′, 68°33′	4950	ss/g	356		3.67	6.9	–		4.13	58.7
Altiplano, Bolivia											
Viscachani	17°10′, 67°58′	3900	s/g	36	6.5–7	0.48	3063	–	3.9892	0.48	6.2
Viscachani (R)	17°10′, 67°58′	3900	s/g			0.59	1646	–		0.592	7.8
Berenguela (A)	17°17′, 69°14′	4100	s/g			3.88	352	–		3.89	55.3
Turco (A)	18°07′, 68°14′	3960	s/g	>20		3.36	210.6	–		3.37	47.8
Pazna	18°35′, 66°55′	3750	s/w	57	6.5	0.62	159.5	1.15	1.5441	0.62	8.2
Pazna (R)	18°35′, 66°56′	3810	s/g	61		0.82	306	–		0.821	11.1
Salinas (R)	19°38′, 67°40′	3720	s/g	9		5.53	2863	–		5.53	78.9
Salinas (A)	19°38′, 67°40′		s/g			6.13	24394	–	4.854	6.133	87.5
Orkohoma (R)	19°12′, 68°27′	3660	s/g	19		2.66	14	–		2.788	39.4
Uyuni N1 (R)	19°38′, 67°37′	3690	s/g	12		3.53	502	–		3.532	50.1
Uyuni N2 (A)	19°38′, 67°37′		s/g			4.19	87.1	–		4.214	59.9
Rio Mulatos	19°43′, 66°46′	3820	s/g	14	6–6.5	1.72	0.89	–		(>1.72)	24.0
Rio Mulatos (R)	19°42′, 66°47′	3780	s/g	13–14		1.39	68	–		1.391	19.3
Sol de Mañana	22°25′, 67°46′	4700	s/g	85	6	2.21	76.68	–	4.7887	2.23	31.4
Sol de Mañana (R)	22°26′, 67°45′	4700	s/g			1.98	217	–		1.98	27.8
Eastern Cordillera, Bolivia											
Tarapaya	19°28′, 65°43′	3350	s/g	57	7–7.5	0.57	78.73	–	1.9641	0.56	7.4
Tarapaya (R)	19°28′, 65°43′			60		0.71	1376	–		0.712	9.5
Chaqui	19°37′, 65°34′	3620	s/w	69	7	0.4	32.11	0.41	1.8342	0.38	4.8
Chaqui (R)	19°37′, 65°34′		s/g	70		0.29	673	–		0.285	3.4

Samples marked with (R) were analysed in the Rare Gas Laboratory, University of Rochester; those marked with (A) were analysed in the laboratories of the Faculty of Earth Sciences, Vrije Universiteit, Amsterdam; also listed are nearby samples from Hoke *et al*. (1994), analysed in the Institut für Mineralogie, FR Geochemie, Freie Universität, Berlin. Analytical details have been given by Hoke *et al*. (1994, 2000) (Berlin and Amsterdam laboratories) and Poreda & Farley (1992) and Giggenbach & Poreda (1993) (Rochester laboratory). Sample type: s, geothermal spring; f, fumarole; fs, flank sulfatara; ss, summit sulfatara; w, water sample; g, gas sample. *T* is the maximum temperature measured at the source of the spring. pH of water was measured above the source. R/R_a is the $^3He/^4He$ ratio R normalized to the atmospheric helium isotope ratio R_a (1.4×10^{-6}). X, sample He/Ne ratio normalized to the calculated air He/Ne ratio at the estimated altitude of recharge of *c*. 4000 m (air $^4He/^{20}Ne = 0.421$), multiplied by 1.322, which is the ratio of the Bunsen solubility coefficients of Ne to He at the estimated recharge temperature of 0 °C. [He]C, helium concentration measured in water samples only; c.CO_2, concentration of CO_2 in sample. R_c/R_a is R/R_a corrected for air contamination (see Hoke *et al*. 1994). % Mantle helium is the calculated percentage of mantle helium, based on the assumption that mantle-derived helium has R_c/R_a of seven and that the measured production ratio of average continental crustal helium is 0.05.

edge effects, the same data are presented in Figure 3b using a contouring routine that is confined to where the data points are actually located. We also show a transect of R/R_a (Fig. 4) in the region of the densest data point distribution at 20 ± 1.5°S, extending across the Andes from the fore-arc in the west into the Eastern Cordillera further east.

We can describe the pattern of helium isotopes in terms of helium essentially produced in the crust ($R < 0.5\ R_a$; see the next section), referred to here as the crustal helium domain, and helium with a significant mantle component ($0.5–7\ R_a$), referred to as the mantle helium domain. The general picture is of a broad mantle helium domain, extending from just west of the active volcanic arc, across the Altiplano and well into the Eastern Cordillera, bounded by crustal helium domains in the west and east. In the Altiplano, the helium isotopic signature is generally above $2.5\ R_a$, reaching $6\ R_a$ in the central part of the Altiplano at Salinas, between the Salar de Coipasa and Salar de Uyuni (Fig. 3a, Table 1). Along the volcanic arc, mantle helium 'highs' are evident (shown by asterisks in Fig. 3b).

The large areal extent of the mantle domain points to a lithospheric-scale explanation for the helium isotopic signature.

Helium and topography

A striking feature of Figure 3a and b is that the shape of the helium contours mimics the general shape of the Andes themselves. For example, the $1\ R_a$ contour clearly follows the marked bend in the Andes at *c*. 17°S, and the high plateau of the Altiplano coincides with the regions where high R/R_a values have been measured. In detail, emissions below 3000 m are characterized by nearly pure crustal helium, whereas those at elevations >3600 m have a strong mantle helium component (Figs 3 and 4). The simplest explanation for this pattern is that those regions at altitudes >3000 m are underlain by mantle that is in a thermal state that allows some mantle helium degassing, most plausibly because mantle melts and mantle melt extraction occur at depth.

Lateral advection and/or crustal sources of helium, discussed below, do not seem to affect this straightforward interpretation of helium data, although they might be enough to slightly elevate the background crustal helium isotopic ratio above a pure crustal ratio *c*. $0.01\ R_a$. We infer that $0.5\ R_a$ is a sensible cut-off value, delimiting the extent of helium truly derived from an underlying mantle melt zone or magma.

Crustal contamination

There are two observations that allow us to argue against lateral advection of helium by groundwater systems in the crust. First, the mantle helium signature in the centre of the Altiplano is higher than anywhere else (Fig. 4); if all the mantle helium here had been transported in shallow groundwater systems down

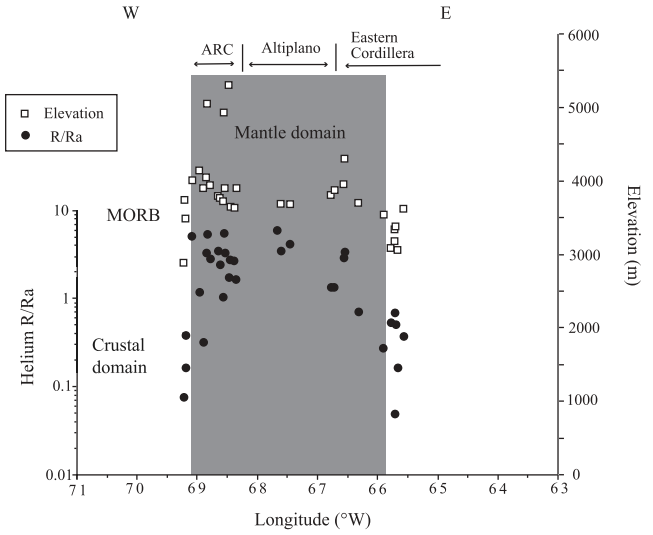

Fig. 4. Helium isotopic analyses for natural helium emissions, expressed as normalized $^3He/^4He$ (R/R_a; see text), plotted against longitude for an east–west transect in a swath 1.5° either side of 20°S. The elevation of helium emissions is also shown. High R/R_a values, >0.5, define a broad region extending from just west of the volcanic arc into the Eastern Cordillera *c*. 300 km farther east, where helium derived from the mantle dominates the helium isotopic signature. It is clear that not only are high R/R_a values confined to the topographically highest points, but also very low values are found at topographically low points, where there are steep topographic gradients. These results suggest that advection of helium by flowing ground waters does not play an important role in determining the mantle helium signature.

topographic gradients from volcanically active areas, then we would expect it to be diluted by crustal radiogenic helium and show a lower mantle component compared with the volcanically active areas. Second, there is no evidence for significant horizontal advection of mantle helium from the volcanic arc into the fore-arc in northern Chile, where topographic gradients are the steepest (*c*. 2° westward): nearly pure crustal helium is found only a few tens of kilometres west of the arc, near the foot of the slope of the high Andes (Fig. 4). Thus, although it is possible that helium emissions with only a small mantle helium component (R/R_a <0.5) could be significantly affected by lateral advection in groundwater systems, helium emissions with R/R_a >1 can only plausibly be explained by a local (*c*. tens of kilometres scale) and deeper source of mantle helium. It is possible that advection of helium is taking place by lateral movement of basaltic magma itself, in either the crust or the mantle. Lateral movement of magma along horizontal conduits away from a magma chamber, if only to a limited degree (not more than a few tens of kilometres), cannot be ruled out.

Another important question is whether the mantle ^3He component is derived from a recent or active melt zone at depth, or has been leached by hydrothermal fluids from older mantle-derived igneous intrusions lodged within the crust. It has been shown (see discussion by Hoke *et al*. 2000), that even if such intrusive bodies were made of pure olivine, they would have to be of the order of tens of kilometres thick to raise the ^3He concentration in ground waters to such an extent as to maintain the observed helium isotopic ratios >1 R_a for more than a million years. This is because the principal carrier phases of helium in rock, such as mafic phenocrysts or the glassy matrix, are prone to alterations and secondary mineralization, and in general have no long-term stability to act as mantle host phases. Likewise, Hilton *et al*. (1998), using an example from the Icelandic hotspot, argued strongly against a contribution of mantle helium to the mantle volatile flux from leached old reservoir rocks. They showed that there is a gross mass imbalance between potential availability and observed concentrations of a mantle helium component in the fluids analysed. Thus, although we cannot rule out older igneous bodies as a source of some of the ^3He in the helium emissions, a recent or active mantle melt zone at depth is a more plausible explanation for the observed elevated helium isotopic ratios >1 R_a.

Helium in olivine megacrysts

A further way to test the previous conclusions is to compare the helium isotopic signature of geothermal gas emissions with that of helium trapped in fluid inclusions in millimetre-sized olivine megacrysts in young basalts (Table 2). The helium isotope ratio in these fluid inclusions is likely to be similar to the helium isotope signature of the host magma and the melt-source region. Thus, if the helium in the gas emissions has not been scavenged in the crust, or undergone advection and mixing, it should have an isotopic signature similar to that of the primary magmatic helium in the fluid inclusions. Ignoring the effects of any subsequent radiogenic helium contribution via crustal contamination, or radiogenic in-growth from the decay of U and Th series elements with time, we would expect a helium isotopic ratio *c*. 8 R_a for a typical mid-ocean ridge basalt (MORB) source (Graham 2002).

Olivine phenocrysts were hand picked from samples collected from young volcanic centres, a few hundred thousand years old, including two maar samples from the Bolivian Altiplano, (Maar 1, Maar 2, Table 3, Fig. 6a) and a dated basaltic andesite flow (0.205 ± 0.024 Ma, Wörner *et al*. 1988) from the active volcanic arc in northernmost Chile, on the northern flank of Pomerape Volcano. Helium was extracted from olivine fluid inclusions by off-line vacuum crushing, following the procedure described by Hilton *et al*. (1993). The results show a narrow range of R/R_a between 6.75 and 7.02 (Table 2), which is close to the observed MORB range (Ozima & Podosek 2002), and only slightly higher

Table 2. *Helium isotopes in fluid inclusions in olivine phenocrysts within Plio-Pleistocene mafic volcanic centres*

Basalt sample locality	Weight (mg)	R/R_a	[He] (ncm^3 STP g^{-1})	% Mantle helium*
Maar-2 (Jaya Kkota)	858	6.86 ± 0.16	20	>84
Maar-1 (Nekhe Kkota)†		6.9		>86
POM (Pomerape)	580	6.75 ± 0.21	11	>82

*Assuming a MORB source with $^3He/^4He$ of 8 R_a.
†Reported by Hoke *et al*. (1994).

Table 3. *K/Ar data for minor mafic volcanic centres in Bolivia and northern Chile*

Sample	Location	Long. (deg.)	Lat (deg.)	K (%)	Error (%)	Wt for Ar (g)	Atmos. ^{40}Ar (%)	Atmos. ^{40}Ar (nl/g)	Rad. ^{40}Ar (%)	Error (%)	Age (Ma)	Error (Ma) ($\pm 2\sigma$)
Volcanic arc (Western Cordillera)												
Gu-3	Flow, SW V. Guallatire	69.1133	18.4666	1.19	1	2.0249	38.08	1.5	1.205	1.22	25.9	0.8
El Rojo 1	Cinder cone, SW V. Irrutupuncu	68.6033	20.9	2.06	1	2.0346	68.65	1.12	0.2514	2.44	3.14	0.17
Northern Altiplano												
R93-9A2	Cone, SW Cerro Pasa Willkhi, SE V. Sajama	68.5916	18.3166	1.96	1	2.065	71.84	1.37	0.2607	2.77	3.43	0.2
R93-11	Flow, E of Laguna Sacabaya	68.7333	18.3166	2.2	1	2.1155	72.85	1.44	0.2535	2.89	2.97	0.18
Bc-5	Flow, NE of Oruru, Banos Capachos	67.02	17.9166	3.72	1	2.013	73.03	3.97	0.7282	2.93	5.04	0.31
Az8	Sill, N of Turco	68.2	18.15	1.05	1	2.0557	50.69	1.84	0.8701	1.44	21.2	0.7
Central Altiplano												
Hui-1	Parinuyo, flow, S of Est. Chullunquiani	67.62	19.0666	1.61	1	2.0448	95.4	1.69	0.0432	19.99	0.69	0.28
Hui-3	Parinuyo, flow, S of Est. Chullunquiani	67.6333	19.0833	1.99	1	2.043	96.41	1.05	0.0192	28.09	0.25	0.14
Maar-1, Bomb C	Nekhe Kkota	67.4516	19.4833	1.68	1	2.4509	98.03	2.04	0.0167	55.64	<0.128	
R93-19	Flow, Estancia Luca, S of Salar de Coipasa	67.95	19.5666	1.55	1	2.1179	89.34	2.75	0.1548	8.66	2.57	0.45
R93-31	Flow, Santuario de Quillacas	66.9366	19.2333	2.59	1	2.14	98.15	1.2	0.0106	57.12	<0.056	
Luk-1	Sill, Chiar Kkollu	67.3633	19.4166	1.09	1	0.7144	48.63	1.076			25.2	0.9
TT-Cia	Tambillo sill, W of Rio Mulatos	67.1483	19.7166	2.62	1	2.066	28.09	1.95	2.4191	1.08	23.6	0.7
R93-26A	Tambillo sill near lower contact at Rodeo	67.2166	19.5166	2.15	1	0.8058	68.56	1.94			23.1	1.2
Altiplano west of Salar de Uyuni												
7/91-19	Flow, N Salar de Empexa	68.3333	20.1166	1.25	1	2.0561	77.65	1.15	0.1616	3.69	3.31	0.25
Pus-2	Flow, SW Salar de Empexa	68.5833	20.4783	1.43	1	2.2045	88.44	1.43	0.0843	7.91	1.52	0.24
Altiplano SW of Salar de Uyuni												
CCO-1 bomb	Scoria cone, Cerro Colorado, E Est. Abaroa	68.0666	21.1	0.85	1	2.0535	74.6	1.02	0.1694	3.14	5.15	0.34
7/91-8	Flow, Chiguana tranca	67.9583	21.05	1.47	1	2.129	87.48	3.39	0.2282	7.28	3.99	0.59
Cav-2	Flow, Cerro Luntapa	67.825	20.9666	1.77	1	2.0247	87.45	1.61	0.1142	7.15	1.66	0.24

Samples of the present study, which are now in the Andes Rock Collection at Oxford University Museum of Natural History. See Kennan *et al*. (1995) for analytical details.

than that for helium emitted in CO_2-rich springs on the Altiplano, not far from the volcanic centres themselves (for example Salinas with R/R_a 5.5–6.1, Table 1). This is strong evidence that the helium collected in the mineral-water springs has taken a more or less direct route from the mantle, up through 65 km of crust, with very little interaction with radiogenic crustal helium. We therefore assume, as a reference value, a mantle helium signature of *c*. 7 R_a for the mantle beneath the Andes, similar to the highest helium ratio measured in the olivine phenocrysts (Table 2). This is consistent with an inferred slight lowering of mantle $^3He/^4He$ in subduction settings compared with a typical MORB source, although there might also be some additional spatial variability (Dodson & Brandon 1999; Martelli *et al*. 2004).

Mafic volcanic centres in the Altiplano

Along with ^{3}He emissions, mafic magmatic activity is an important manifestation of mantle melting. The distribution and geochemistry of young volcanic activity, such as the Plio-Pleistocene centres in the Bolivian Altiplano, can be compared directly with the helium emissions. Older Cenozoic mafic volcanic activity and shallow intrusions in the Altiplano, and western margin of the Eastern Cordillera, constrain the longer-term history of mantle melting and lithospheric evolution in the region.

First we characterize the regional and temporal distribution and geochemistry of the mafic magmatism, then we attempt to constrain the depth range of their melt source regions.

Distribution, geochemistry and timing

Figure 5 shows the locations of basalts and basaltic andesites analysed in this study (now in the Andes Rock Collection at Oxford University Museum of Natural History), which crop out between 17°S and 22°S, and usually are easily identified in satellite images. Plio-Pleistocene volcanic centres are distributed regionally from the active volcanic arc, in the west, to up to 200 km farther east, across the Altiplano high plateau region. They form monogenetic centres, lava flows, cinder cones and maars. Oligo-Miocene mafic volcanic rocks and shallow intrusive rocks mainly crop out on the eastern margin of the Altiplano, either as lava flows (often pillowed and interlayered with tuffs) or forming regional shallow-level stratiform sills in the deformed Miocene to Oligocene red-bed successions exposed on the Altiplano.

The behind-arc volcanic rocks have a compositional range similar to that found in the arc (Thorpe *et al*. 1984; Davidson & de Silva 1992, 1995). The Oligo-Miocene samples in this study are basalts and shoshonites, whereas the Plio-Pleistocene samples are mainly basalts or high-potassium basaltic andesites (Fig. 6).

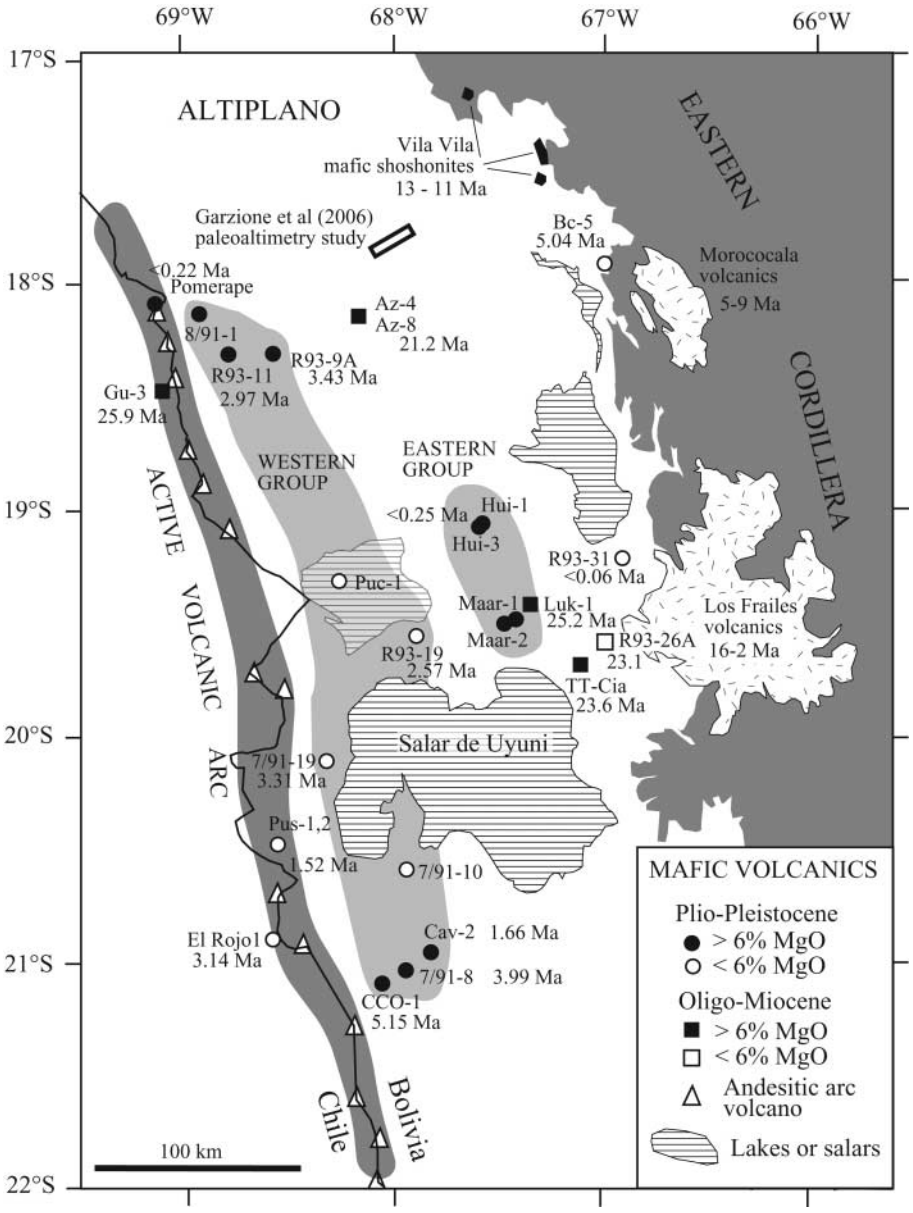

Fig. 5. Location and ages of Oligo-Miocene and Plio-Pleistocene mafic volcanic centres analysed in this study, which crop out in the Altiplano. The active volcanic arc runs along the border between Chile and Bolivia. (See Fig. 1 for location of box.) Monogenetic mafic volcanic centres were dated as part of this study using the K–Ar technique. Plio-Pleistocene centres (<5.15 Ma), with MgO >6% were analysed in two groups, located on the western (Western Group) and eastern (Eastern Group) margins of the Altiplano. Also shown are the locations of extensive 16–2 Ma ignimbrites and dacitic volcanic rocks, as well as 13–11 Ma mafic shoshonitic eruptions, on the eastern margin of the Altiplano and western margin of the Eastern Cordillera. The palaeoaltimetry study by Garzione *et al*. (2006) was carried out on a Late Miocene sedimentary sequence in the Corque syncline, in the northern Bolivian Altiplano.

Major and trace element chemical analyses are listed in Table 4, and are summarized in Figs 6 and 7.

K/Ar ages for mafic magmatic rocks presented in this study (Table 3, Fig. 5; see Kennan *et al*. 1995, for analytical details) generally fall into two periods: a younger phase, less than *c*. 5.2 Ma (mainly <3.5 Ma), and an older Oligo-Miocene phase between 21 and 25 Ma (see also Hoke *et al*. 1993). However, felsic–intermediate–mafic magmatism in the Altiplano (Baker & Francis 1978; Redwood & MacIntyre 1989; Wörner *et al*. 2000; this study), and western margin of the Eastern Cordillera (Fig. 8; Evernden *et al*. 1977; Grant *et al*. 1979; Schneider 1985; Kennan *et al*. 1995; Barreiro *et al*. 1999; Barke 2004), continued throughout the intervening period. In particular, extensive shoshonitic eruptions occurred in the northern Altiplano at 13–11 Ma (Figs 1, 5 and 8; Redwood & MacIntyre 1989).

At *c*. 25 Ma, after a *c*. 10 Ma period of magmatic quiescence, mafic to felsic magmatism between 16°S and 22°S abruptly flared up right across the high Andes, extending to 300 km behind the arc (Fig. 8). Soon afterwards, large volumes of ignimbrites (Oxaya Formation) were erupted in the arc between 22 and 19 Ma (Wörner *et al*. 2000), followed by the emplacement of mafic arc shield volcanoes between 18.5 Ma and *c*. 6 Ma (Wörner *et al*. 2000). However, by *c*. 3 Ma, the volcanic arc had narrowed to its present width (Wörner *et al*. 2000). Throughout this period, there is no clear indication of any marked phases or pattern in the behind-arc magmatism, except for a westward migration up to *c*. 50 km of the eastern limit (Fig. 8).

The Plio-Pleistocene mafic centres show no clear relation between age and location. We divide them into a Western Group, which crops out in a region extending from the active volcanic to 75 km farther east, and an Eastern Group, which crops out 100–200 km east of the active arc (Fig. 5). The Oligo-Miocene mafic volcanic rocks crop out predominantly more than 100 km behind the arc at that time.

Our work expands on and complements a previous study of late Cenozoic magmatism in the Bolivian Altiplano by Davidson

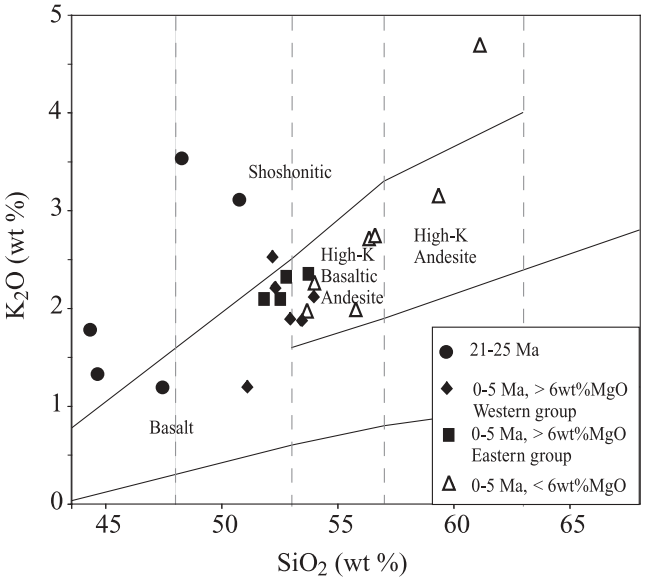

Fig. 6. Classification of mafic back-arc volcanic rocks analysed in this study (after Taylor *et al*. 1981). Less evolved samples of the Oligocene–Miocene group plot in the shoshonitic field, whereas the Plio-Pleistocene samples are of high-K calc-alkaline type.

& de Silva (1992, 1995), increasing both the area of study and the number of samples. Their study focused on the Plio-Pleistocene volcanic rocks of the Altiplano and arc stratovolcanoes.

Constraining the depth of the melt zone

The depth and extent of the melt region is a crucial parameter in any attempt to constrain the origin of mantle melting beneath the high Andes. Here, we use the approach of McKenzie & O'Nions (1991) to explore this further, based on the REE concentrations in a selected group of mafic volcanic rocks (MgO >6%, see the section 'Sample grouping'). This is a geochemical inverse method, rather than a physical forward model of melting and melt extraction. (McKenzie 1984; Klein & Langmuir 1987; McKenzie & Bickle 1988; Watson & McKenzie 1991), reconstructing the source region from the composition of resultant magmatic rocks (Kay & Gast 1973; Minster & Allègre 1978; Albarède 1983; Hofmann & Feigenson 1983). An important additional constraint is that mantle melting must occur at depths greater than the crustal thickness.

REE modelling

McKenzie & O'Nions (1991) have used inverse theory to calculate the distribution of melt fraction with depth of the mantle melt zone required to produce the REE concentrations in mafic magmatic rocks. The technique has been investigated for a wide range of volcanic environments, including mid-ocean ridges, oceanic islands, island-arcs and continental volcanic rocks (McKenzie & O'Nions 1991, 1995, 1998; Pearce & Parkinson 1993) with results that make sense in terms of the existing understanding of the physical processes of melting, melt extraction and potential melt source regions. We make use of this experience in the application of the method of McKenzie & O'Nions (1991) to the behind-arc mafic volcanic rocks of the Central Andes. The method has been described in full by McKenzie & O'Nions (1991), and here we briefly review some of the basic assumptions. Only REE concentrations are used for the inversion procedure because, with their low concentrations, their activities in both melt and residue should be proportional to their concentrations, so their distributions between melt and matrix can be described by a partition coefficient using Henry's Law, and their concentrations in volcanic rocks are generally well determined (McKenzie & O'Nions 1991).

The important assumption is that mantle nodules can be used to determine the mineral composition in the mantle source region, assuming a Bulk Earth mantle composition (McKenzie & O'Nions 1991; but see below), which we compare and contrast with the MORB source. We assume that REE concentrations in the melt will be primarily determined by the presence of plagioclase, or spinel, or garnet in the melt source; these minerals will strongly affect the REE partitioning into the melt phase, and their presence is largely controlled by pressure/depth. Given a potential temperature for the mantle, and an adiabatic geotherm, the depth of the stability field for these minerals can be defined. In our analysis, we assume a MORB environment with a potential temperature of 1300 °C, and typical mantle densities, so that the stability fields are as follows: spinel-in *c*. 25 km, plagioclase-out *c*. 35 km, garnet-in *c*. 60 km, spinel-out *c*. 80 km. The inversion assumes a 1D vertical model of fractional melting, in which the melt is extracted as it is formed from a simple vertical column. Finally, the effects of fractional crystallization of the melt are assumed to be small and are ignored.

It could be argued that the composition of the melt is strongly affected by fluids derived from the subduction zone. However, Hawkesworth *et al*. (1991) used trace element and isotope geochemistry of arc magmas to infer that the fluid flux from the slab into the melt source region accounts for <15% of certain large-ion lithophile elements (LILE) such as Sr. In addition, fluid migration is likely to have a relatively small effect on the concentrations of the more immobile heavy REE (HREE) (Pearce 1983, Davidson 1996). The HREE concentrations are an important constraint in our analysis, because their partition coefficients between garnet and the melt phase are an order of magnitude or more greater than the partition coefficients with respect to spinel or plagioclase (McKenzie & O'Nions 1991). Thus, the HREE concentrations in the melt are sensitive to whether partial melting has taken place predominantly in garnet peridotite below *c*. 80 km, or in spinel- or plagioclase-bearing peridotites at shallower depths. These depths are calculated for a MORB environment and have to be recalculated for the presence of various thicknesses of continental crust.

In any case, we can allow to some extent for enrichment or metasomatism of the mantle source region by considering the effect of the addition of small melt fractions from a MORB source (McKenzie & O'Nions 1995), which might be expected to have many of the geochemical characteristics of fluids derived from subducted oceanic crust. For example, REE concentrations that are greater than those predicted by melting of a simple MORB source or primitive source have been commonly observed for continental volcanic rocks and some ocean islands where melting has involved only small melt fractions (McKenzie & O'Nions 1991, 1995, 1998; Tainton & McKenzie 1994). McKenzie & O'Nions (1991) suggested that, in some cases, these could be explained by the presence of amphibole in the source region, during wet melting, but subsequent analysis suggests that a simple enrichment of the source with a small melt fraction of the MORB source is a better explanation of the observed trace element enrichments (Tainton & McKenzie 1994; McKenzie &

Table 4. *Major (wt%) and trace element (ppm) and isotopic compositions for Plio-Pleistocene and Oligocene–Miocene mafic volcanic rocks and intrusions in the Altiplano back-arc region*

	Plio-Pleistocene Western Group						Plio-Pleist. Eastern Group				Plio-Pleistocene <6% MgO							Oligo-Miocene (25–21 Ma)				
	8/91-1	R93-9A2	R93-19	CCO-1 bomb	7/91-8	Cav-2	Hui-1	Hui-3	Maar-1 bomb C	Maar-2	R93-11	7/91-19	Pus-1	Bc-5	R93-31	7/91-10	Puc-1	Luk-1	Az-4	Gu-3	TT-Cia	R93-26A
SiO_2	52.27	52.17	53.01	51.06	53.4	53.98	52.52	53.77	52.85	51.85	56.33	53.68	55.73	61.12	59.33	53.97	56.58	44.66	47.49	44.36	48.28	50.77
TiO_2	1.49	1.89	1.59	0.93	0.99	1.32	1.4	1.38	1.44	1.41	1.35	1.69	1.05	1.71	1.07	1.25	1.48	2.28	1.62	0.92	1.22	0.97
Al_2O_3	15.92	15.13	15.29	15.47	15.35	15.78	16	15.92	15.88	15.79	15.22	16.49	17.34	14.08	15.72	17.26	16.12	13.72	12.65	11.52	16.4	19.71
Fe_2O_3	3.99	9.45	8.92	3.05	2.05	9.1	2.33	1.14	8.6	8.88	7.65	3.06	7.56	1.59	6.56	3.43	2.94	3.76	11.66	9.76	10	7.22
FeO	5.26			5.97	6.41		5.97	6.76				4.89	0	4.09		4.39	3.86	6.99				
MnO	0.15	0.13	0.12	0.15	0.14	0.14	0.14	0.13	0.15	0.15	0.1	0.11	0.11	0.07	0.1	0.12	0.1	0.18	0.17	0.18	0.18	0.13
MgO	6.23	6.34	7.85	9.06	7.94	6.31	7.63	7.18	7.02	7.28	5.85	5.69	4.05	2.9	5.49	4.29	4.01	9.39	12.69	14.87	6.6	2.92
CaO	8.22	7.58	7	9.17	7.02	7.02	8.12	7.14	8.23	8.65	6.19	7.45	7.24	3.87	5.53	7.67	6.02	12.16	8.63	10.13	8.68	7.03
Na_2O	3.01	4.13	3.95	2.76	3.01	3.78	3.14	3.15	3.54	3.46	3.91	4.15	3.89	3.02	2.83	3.84	4.45	3.06	2.78	4.53	3.65	4.71
K_2O	2.23	2.52	1.88	1.19	1.86	2.12	2.08	2.34	2.32	2.11	2.7	1.95	1.97	4.7	3.14	2.24	2.73	1.32	1.19	1.78	3.53	3.12
P_2O_5	0.44	0.87	0.52	0.19	0.27	0.37	0.37	0.35	0.42	0.4	0.53	0.56	0.25	0.87	0.3	0.4	0.54	0.73	0.52	0.58	0.76	0.69
LOI	0.89	−0.05	0.17	1.07	1.19	0.19	0.92	0.78	0.07	0.33	0.59	0.61	1.35	1.86	−0.07	0.8	1.11	1.85	0.88	1.7	1.03	2.94
Total	100.1	100.16	100.29	99.97	99.63	100.12	100.62	100.32	100.53	100.29	100.42	100.33	100.54	99.89	100	99.66	99.93	100.1	100.27	100.33	100.33	100.21
Rb	37	49	29	26	46	46	49	60	55	48	46	29	37	147	111	52	49	20	24.6	46.4	66.2	49.3
Sr	961	1396	969	390	745	798	614	594	776	751	1061	977	629	781	511	1090	1192	876	871	1516	1092	1447
Ba	963	1445	854	362	621	991	752	940	887	761	1283	907	607	1489	1096	1031	1319	624	512	835	809	1174
Ga	21	23	24	17	18	21	22	23	23	23	22	24	20	24	25	21	24	19	18	16	19	20
Y	30	21	13	20	30	25	23	24	23	23	15	17	19	29	23	22	16	25	21	19	28	21
Zr	188	312	202	108	136	186	172	183	206	186	255	224	132	356	195	201	242	186	190	163	226	201
Nb	12	26	16	10	14	13	23	25	32	27	13	24	8	31	21	18	19	60	22	15	22	15
Cr	135	171	297	727	333	147	365	333	257	298	150	175	48	99	185	20	91	387	567	825	245	16
Ni	49	101	164	114	62	42	87	89	92	84	164	69	23	39	34	18	37	119	359	423	92	15
Pb	–	7	6	–	–	8	–	–	9	7	9	–	–	–	17	–	–	–	5	7	13	9
Cu	45	30	45	44	25	29	47	44	55	46	50	45	65	27	21	19	28	85	67	129	155	83
Zn	101	112	115	90	96	126	92	101	90	90	101	105	91	104	101	99	105	94	106	89	80	62
Sc	–	17	17	–	–	21	–	–	22	26	16	–	–	–	17	–	–	–	19	26	22	13
V	249	217	192	229	207	220	216	200	222	233	160	198	176	107	150	195	144	264	206	200	247	174
La	36.9	73	21.3	13.2	25.8	34.2	34.7	34.6	34.3	31.1	46.7	37.1	18.5	72.6	43.6	40.2	49.9	49.7	39.4	47.5	43.8	45.7
Ce	78	151	46	30	56	74	68	71	70	64	96	81	40	149	84	81	103	96	84	99	88	94
Pr	9.9	17.6	5.9	3.9	7.1	9.3	8.6	8.8	8.4	7.4	11.3	10.1	5.3	17.3	9.7	9.8	11.9	11.5	10.3	12.2	10.4	11
Nd	39.9	67.1	23.9	15.9	28.8	38.5	34.7	35.3	32.9	30.4	44.2	42.2	21.9	66	37.6	37.5	46.3	46.4	41.5	46.4	41.4	43.1
Sm	7.25	12	4.73	3.63	5.58	7.72	7.54	6.73	6.13	6.28	7.96	8.38	4.59	11.58	7.31	6.84	7.7	8.76	7.59	7.91	7.99	8.11
Eu	2.25	3.1	1.37	1.06	1.49	2	1.79	1.99	1.84	1.74	2.19	2.33	1.31	2.89	2.12	1.78	2.24	2.87	2.45	2.02	2.27	2
Tb	1.01	1.06	0.52	0.61	0.87	0.89	0.92	0.86	0.87	0.79	0.76	0.78	0.6	1.13	0.92	0.78	0.72	1.03	0.96	0.76	1	0.92
Gd	7.18	8.81	3.82	3.67	5.71	6.72	6.39	6.28	5.99	5.78	5.93	6.47	4.42	9.42	6.15	5.7	5.72	8.37	6.86	6.24	7.25	6.67
Dy	5.56	5.39	2.57	3.6	5.79	4.96	5.02	4.88	4.63	4.58	3.99	4.02	3.78	6	4.69	3.96	3.44	5.72	4.91	4.19	5.27	4.54
Ho	1.06	0.86	0.47	0.71	1.13	0.89	0.94	0.88	0.87	0.82	0.66	0.63	0.69	0.94	0.9	0.7	0.58	0.98	0.85	0.74	0.96	0.8
Er	3.06	2.08	1.07	2.29	3.42	2.75	2.45	2.35	2.16	2.4	1.69	1.48	1.93	2.3	2.35	1.91	1.32	2.32	2.17	1.95	2.85	2.3
Tm	0.41	0.29	0.12	0.3	0.48	0.37	0.31	0.29	0.29	0.3	0.24	0.24	0.31	0.3	0.36	0.25	0.19	0.31	0.29	0.27	0.36	0.29
Yb	2.57	1.7	0.87	1.99	2.82	2.32	2.07	2.07	2.06	2.02	1.36	1.29	1.68	1.84	2.11	1.74	1.09	2.06	1.7	1.81	2.36	1.9
Lu	0.36	0.21	0.13	0.31	0.43	0.35	0.27	0.29	0.27	0.28	0.21	0.18	0.24	0.27	0.31	0.26	0.15	0.27	0.24	0.27	0.35	0.29
Hf	6.09	8.83	4.65	3.86	4.32	5.64	5.79	6.09	6.19	5.71	7.28	6.45	4.07	10.27	5.24	5.39	7.21	5.49	6.06	3.92	6.09	8.18
Ta	0.86	1.54	0.86	1.65	0.98	1.1	1.65	1.59	3.05	2.35	0.81	1.28	0.59	1.33	1.13	0.88	1.1	3.47	1.82	1.16	1.7	1.87
Th	4.04	10.72	1.9	2.54	5.04	4.74	7.18	7.65	7.6	6.31	5.29	3.18	2.99	14.73	7.2	7.9	5.89	5.77	4.36	3.82	8.95	14.63
U	0.67	1.85	0.53	0.9	2.14	2.03	1.52	1.66	1.71	1.4	0.91	0.67	0.8	3.03	1.96	1.61	1.18	1.65	1.02	0.78	2.68	3.56
$^{87}Sr/^{86}Sr$	0.70635	0.706366	–	0.70582	0.70578	–	0.70689	0.70741	0.705961	0.705956	–	0.70555	0.70559	0.70963	0.707955	0.70597	0.70556	0.70396	–	–		–

Samples of the present study, which are now in the Andes Rock Collection at Oxford University Museum of Natural History. REE were analysed by inductively coupled plasma mass spectrometry at NERC Isotope Geosciences Laboratory, Keyworth, UK. LOI, loss on ignition.

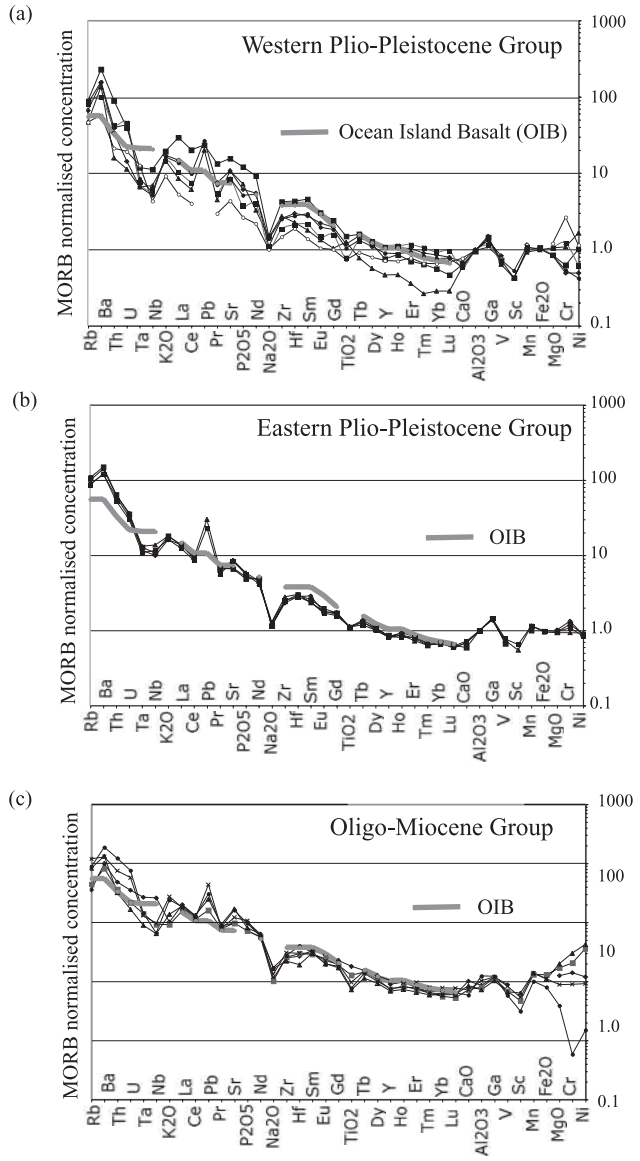

Fig. 7. MORB-normalized spidergrams using the model by Pearce (1983), placing elements in order of relative incompatibility with a fertile spinel lherzolite mantle (Pearce & Parkinson 1993). Plot for average ocean island basalt (OIB) is shown for comparison. The three MORB-normalized spidergrams represent the three groups of mafic back-arc volcanic rocks: (**a**) the western young group (<5.3Ma); (**b**) the eastern young group; (**c**) the Oligocene–Miocene group.

O'Nions 1995, 1998). McKenzie & O'Nions (1995) proposed that this enrichment was a consequence of entrainment of part of the metasomatic thermal boundary layer, defined as the transition zone between the lithosphere or mechanical boundary layer and the convecting asthenosphere, during mantle convection. In some cases, enrichment of HREE in continental volcanic rocks can be best explained by an initial depletion (*c*. 15%) of the source region because of an earlier phase of basalt generation (Tainton & McKenzie 1994).

Sample grouping. We inverted the REE concentrations for both the Plio-Pleistocene and Oligo-Miocene behind-arc mafic volcanic rocks (Table 4, Fig. 9). Only analyses from samples with MgO >6% were used in the inversion procedure, to minimize any effects of low-pressure fractionation. This gave us 10 Plio-Pleistocene samples, and four Oligo-Miocene samples (Table 4, Fig. 5). Separate analysis of the Western and Eastern Groups of Plio-Pleistocene volcanic rocks (Fig. 5) allowed us to investigate variations in the depth of the source region with distance behind the arc, equivalent to a deepening of the subducting Nazca plate from *c*. 120 km to *c*. 250 km.

Modelling procedure. First, the inversion was carried out assuming single-stage melting of a MORB source. Previous modelling has shown that this often does not work well for continental volcanic rocks and predicts trace element concentrations that are significantly lower than the observations (McKenzie & O'Nions 1991, 1995, 1998; Tainton & McKenzie 1994). To deal with this, the two-stage melting model of previous workers (McKenzie & O'Nions 1991, 1995, 1998; Tainton & McKenzie 1994) was used, with the enrichment of the source region with a small melt fraction, produced by melting in the garnet stability field, and recalculating the source mineralogy in the various stability fields, using the mean mineral compositions from all spinel peridotite nodules. This enriched source was then remelted in the inversion procedure. Through trial and error, an enrichment was found that yielded the best fit to the REE pattern and other trace element data.

For the purposes of the inversion, all depths were converted into those of mantle rock columns with equivalent pressures. The mantle melt source region for the western Plio-Pleistocene grouping must occur at depths greater than the underlying 75–80 km thick crust (equivalent to 65–70 km of mantle thickness), potentially in both spinel–garnet and garnet peridotite (Figs 9 and 10). For the eastern Plio-Pleistocene grouping, the mantle melt source must be deeper than the underlying 65 km thick crust (equivalent to 55 km of mantle thickness), with the possibility of some melting in spinel peridotite without garnet (Figs 9 and 10). The mantle melt source region beneath the Altiplano during the Oligo-Miocene (*c*. 25 Ma) must be deeper than the estimated 45–50 km thick crust at that time (Lamb & Hoke 1997), equivalent to a mantle rock thickness of *c*. 40 km. Thus, a significant thickness of spinel peridotite would be available as a potential melt source for the Oligio-Miocene Altiplano volcanic rocks.

Results

Overall, the REE element inversions for all groupings of mafic volcanic rocks require melting of peridotite in the spinel to spinel–garnet transition zone, and thus a significant melt fraction was formed at mantle depths <90 km (Fig. 10; for equivalent mantle thickness (<80 km) see Fig. 9). This is the principal result of our analysis, and it is particularly evident for samples farthest behind the arc, which have REE concentrations that are very similar to those in intraplate ocean island basalts (OIB; McKenzie & O'Nions 1995). The shallow depths are well constrained by the relatively high concentrations of the more immobile HREE, requiring significant partial melting at shallow mantle depths where garnet is not present or in low modal proportions.

Plio-Pleistocene behind-arc mafic centres. The REE inversion results for the Eastern Group of volcanic centres, located between 100 and 150 km behind the arc, show that the REE pattern could not be reproduced by one-stage melting of a MORB source, underestimating the REE from Ce to Eu. However, a

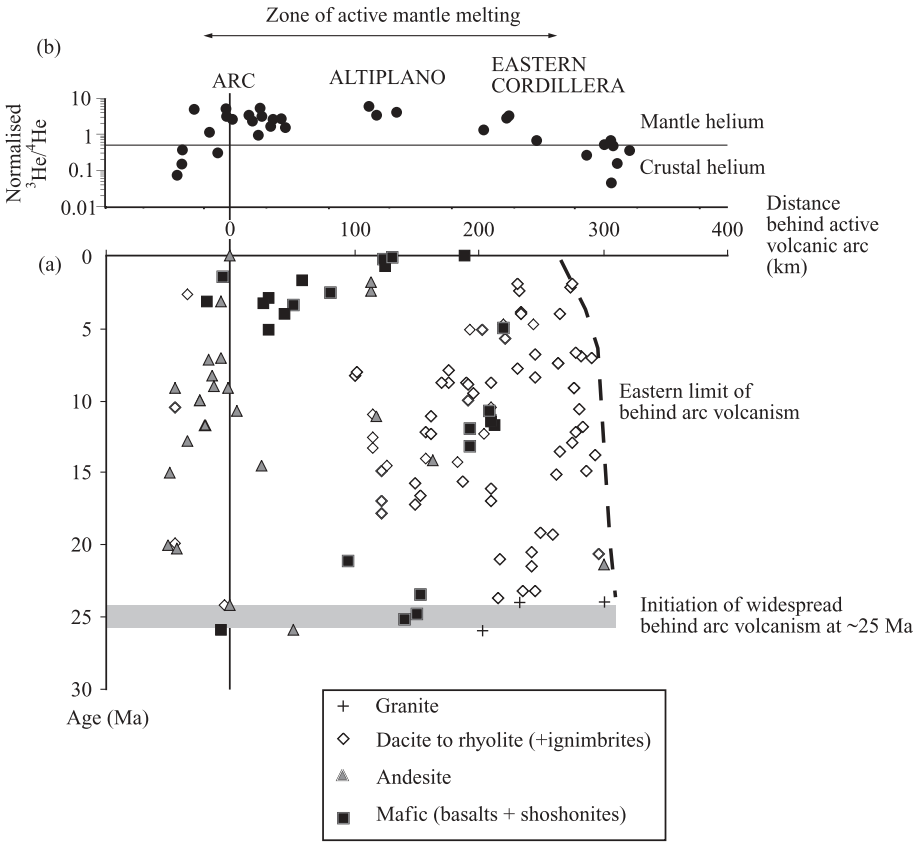

Fig. 8. (**a**) Plot of age against distance perpendicular to the active arc of Neogene volcanic and plutonic rocks in the Andes between 16° and 22°S (compiled from Evernden *et al*. 1977; Grant *et al*. 1978; Schneider 1985; Redwood & MacIntyre 1989; Kennan *et al*. 1995; Barreiro *et al*. 1998; Wörner *et al*. 2000; Barke 2004; this study). Arc and widespread behind-arc volcanism started abruptly at *c*. 25 Ma, after a *c*. 10 Ma period of arc quiescence. Since then, there has been more or less continual felsic to mafic volcanism extending up to *c*. 300 km behind the arc. The *c*. 50 km westward migration of the eastern limit of magmatism should be noted. (**b**) Profile of normalized $^3He/^4He$ in geothermal emissions, showing the pronounced mantle helium signature extending across the high Andes, in the same region where there is behind-arc dacitic–rhyolitic volcanism. This strongly suggests that the heat source for this volcanism is mantle melts at depth in the crust, which only occasionally erupt at the surface as basalts.

simple enrichment of the source region, adding 6% of a melt fraction produced by 0.4% melting in the garnet stability field of a MORB source, when remelted, results in an excellent fit to the REE data (Fig. 9c).

The resultant trace element chemistry and melt fraction distribution is typical of small oceanic islands (see inversion for Inaccessible Island, McKenzie & O'Nions 1998). There is some indication of an island arc signature, because Ti is low, and Rb–U values are high (McKenzie & O'Nions 1991), but it is a very slight effect given the similarities to oceanic islands such as Inaccessible Island. The best-fit melt model requires over 90% of the melting occurs at depths <80 km, within the stability field of the spinel and garnet (Fig. 10b), and right up to the base of the overlying crust (*c*. 65 km), although it is possible that in reality melting terminates up to 10 km deeper, with higher melt fractions somewhere near the base of the spinel zone or near the top of the spinel–garnet transition zone. What is clear is that the REE concentrations of the volcanic rocks cannot be explained by a melt source region that lies only in garnet peridotite, at depths >90 km.

The same melting model was tried on the Western Group of volcanic centres, but does not work well for the HREE Er to Lu (Fig. 9a). This is a common problem with continental volcanic rocks and is most extreme for kimberlites (Tainton & McKenzie 1994). To model these rocks, McKenzie & O'Nions (1995) used initial source depletion followed by enrichment, a process that has been observed in mantle nodules in alkali volcanic rocks (McKenzie & O'Nions 1995). This procedure was carried out for the Western Group, starting with a 15% initial depletion of the MORB source, resulting in good fits for the REE, although we recognize that it is always possible to improve the fit by increasing the number of degrees of freedom in the model, and there may be trade-offs between the effects of enrichment, depletion, and melt depth. However, Rb to U values are still too high and Ta, Nb, P too low for the model (Fig. 9b). This signature is typical for island arcs, but is not found in oceanic islands (McKenzie & O'Nions 1998), suggesting that the Western Group is more influenced than the Eastern Group by the processes that generate arc volcanism, in accord with the much closer proximity of the Western Group to the active volcanic arc (Davidson & de Silva 1995).

The thicker crust beneath the Western Group (75–80 km), compared with the Eastern Group, suggests that the melt source region must be in the spinel–garnet transition zone and underlying garnet peridotite (Fig. 10a). The best-fit model requires significantly higher melt fractions in garnet peridotite, compared with melt generation for the Eastern Group, suggesting that melting in the Western Group extends to slightly deeper depths than farther east. However, >80% of the melt must still be generated at depths <100 km, so that any real difference in the depth of the melt zone for the Western and Eastern Groups may only be relatively small (Fig. 10a).

The inversions for both the Western and Eastern Groups show higher Mg, Cr, Ni and Fe concentrations than is observed (Figs 8 and 10), suggesting some fractionation of the magma. In general, their overall trace element chemistry is very like the behind-arc volcanism in the Aegean (D. McKenzie, pers. comm.), with a similar variation with increasing distance from the Hellenic arc. Given the marked difference in crustal thickness between the Bolivian Altiplano (65–75 km) and the Aegean (*c*. 40 km), we can only conclude that there is no obvious signature of the thick crust affecting the REE in the Bolivian behind-arc mafic volcanic rocks.

Oligo-Miocene behind-arc mafic lavas and sills. The REE inversion results for the Early Miocene behind-arc volcanic rocks and

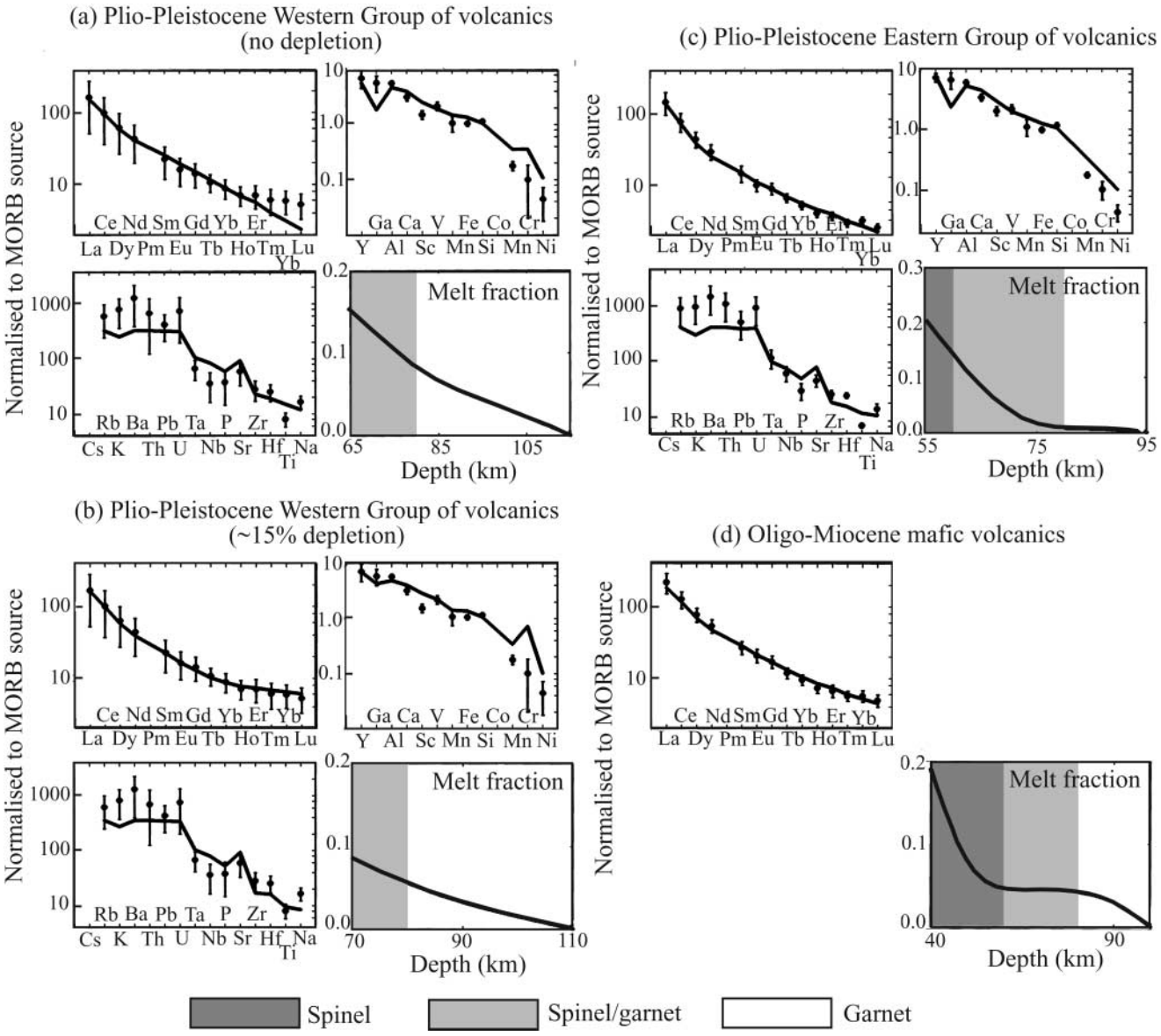

Fig. 9. REE inversion results for behind-arc mafic volcanic rocks. For each grouping, the REE analyses were averaged. The results for each grouping are shown as a cluster of four plots: (1) in the top left-hand corner, the actual REE measurements are plotted (normalized to MORB source), with the inversion result as a continuous line; (2) in the top right-hand and bottom left-hand corners, the measured abundances of other trace elements are plotted, with calculated abundances, based on the melt zone model, shown as continuous lines; (4) in the bottom right-hand corner, the predicted melt zone model, based on the REE inversion, is plotted as melt fraction against depth, with the spinel, spinel–garnet transition, and garnet stability fields marked. (**a**) Western grouping of Plio-Pleistocene mafic volcanic centres, assuming an undepleted MORB source with small enrichment. (**b**) As in (**a**), but for a *c*. 15% depletion of MORB source. (**c**) Eastern grouping of Plio-Pleistocene mafic volcanic centres, with small enrichment. (**d**) Oligo-Miocene behind-arc volcanic rocks, with a small enrichment.

shallow intrusions are very similar to those for the Eastern Group of Plio-Pleistocene volcanic centres, with a small enrichment of the source region required and an excellent fit to the REE data (Fig. 9d). The shallow parts of the melt zone are well resolved, with significant melting in the spinel stability field, and >80% of the melt generated at depths <90 km (Fig. 10c; for equivalent mantle thickness of 80 km, see Fig. 9c). It is particularly interesting that the requirement in the REE inversions for relatively shallow depths in spinel peridotite is consistent with the prediction of thinner crust beneath the Altiplano in the Oligo-Miocene (Lamb & Hoke 1997).

Mechanism for melting beneath the Bolivian Andes

Lithospheric structure beneath the Bolivian Andes

Important for any model of melt generation beneath the Bolivian Andes is the lithospheric structure. Indeed, the main aim of this study has been to use the evidence for mantle melting, combined with an understanding of the processes of melting, to improve the constraints on the lithospheric structure. Figure 11 summarizes our inferred present-day lithospheric structure for the Bolivian Andes at *c*. 20°S. We interpret the sharp cut-off of mantle helium in the west to mark the western limit of the

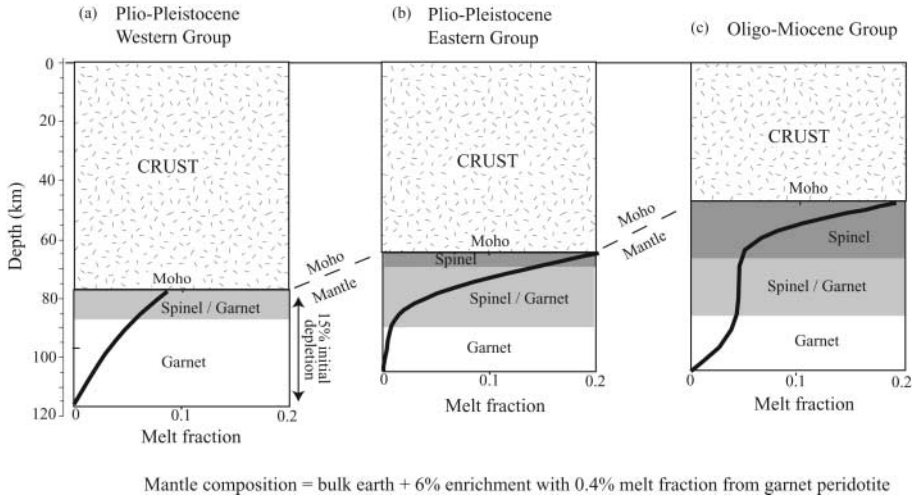

Fig. 10. Mantle melt fractions plotted against depth for the three back-arc volcanic groups analysed in this study: (**a**) Western Plio-Pleistocene Group; (**b**) Eastern Plio-Pleistocene Group; (**c**) Late Oligo-Miocene group, deduced from inversion of the REE (see text).

asthenospheric mantle wedge, lying slightly west of the active volcanic arc. Likewise, we interpret the cut-off, farther east, in the Eastern Cordillera, to mark the western edge of the thick (⩾150 km) lithosphere of the Brazilian Shield, which has been underthrust beneath the Eastern Cordillera. Our lithospheric model, based on evidence for mantle melting, shows remarkable correlation with heat-flow, seismic tomographic and flexural rigidity studies of this part of South America (Henry & Pollack 1988; Whitman *et al*. 1992; Widiyantoro & van der Hilst 1997; Myers *et al*. 1998; Springer 1999; Van der Hilst & Karason 1999; Fukao *et al*. 2001; Van der Lee *et al*. 2001; Watts *et al*. 1995; Stewart & Watts 1997; Black 2000). Thus, the region of high heat flow (Henry & Pollack 1988, Springer 1999) and the 'outer' limits, in the west and in the east, of shallow seismically slow mantle in the tomographic 20°S cross-section of Myers *et al*. (1998), more or less coincide with the boundaries of the zone of helium emissions with a significant mantle component (Fig. 11a, $R/R_a \ll 0.5\ R_a$).

The western seismically slow zone underlies the active volcanic arc, where the depth of mantle melting is constrained by the REE modelling between 75 and 120 km. However, the eastern seismically slow zone, beneath the western margin of the Eastern Cordillera, underlies the region where there have been extensive Miocene to Pleistocene Los Frailes ignimbrite eruptions (*c*. 12 Ma to *c*. 2 Ma; Schneider 1985; Kennan *et al*. 1995; Barke 2004) (Fig. 8). The present-day strong mantle helium signature measured here in mineral-water and geothermal springs, reaching $4\ R_a$ near the village of Tomavi (Hoke *et al*. 1994), suggests that mantle melts, introduced deep in the crust, have provided the heat source for crustal melting (Annen & Sparks 2002) and ignimbrite activity, and that mantle melting is still active beneath this region. Furthermore, surface heat-flow values are in excess of $70\ mW\ m^{-2}$ in this region and are the highest in the Bolivian Andes (James & Sacks 1999).

The helium emissions become essentially pure radiogenic ($R < 0.5\ R_a$) about 50–100 km farther east in the central part of the Eastern Cordillera, where there is no evidence for volcanic activity since the early Miocene, and the fast lid is thicker. Here, the elastic thickness appears to increase rapidly from <25 km at 65°W to *c*. 50 km farther east at 64°W (Black 2000; Fig. 10a) and heat-flow values are around $50\ mW\ m^{-2}$, consistant with shield areas.

The picture is not so clear in the central part of the Altiplano, west of the Los Frailes ignimbrites, where there is a strong mantle helium signature in gas emitted in mineral-water springs, and REE modelling suggests mantle melting at depths between 65 and 90 km, but the Myers *et al*. (1998) tomographic model has a relatively fast 'lid' around 125 km thick. Indeed, the highest helium isotopic ratio measured in the back-arc of the Central Andes comes from the very centre of the Altiplano, near the village of Salinas, between the Salar de Uyuni and Salar de Coipasa. Here, the cold CO_2-rich mineral-water spring at Salinas is emitting helium with an isotopic ratio of $6.13\ R_a$, suggesting that at least 87% of the helium is coming from a $7\ R_a$ mantle source (Table 1, Figs 3 and 4). Thus, if a thicker lithospheric core really exists beneath the central part of the Altiplano, then it is either being permeated by melt conduits leading off the mantle melt regions beneath the Los Frailes ignimbrites and/or the volcanic arc or the incipient mantle melting is 'invisible' to seismic waves.

Focusing of arc volcanism

Arc volcanism in the Central Andes has been remarkably steady through time, giving rise to more or less continuous and mainly andesitic volcanism for the last *c*. 25 Ma, with some migration of the western front and an initial wide east–west distribution narrowing to its present *c*. 50 km wide zone by about 3 Ma (Wörner *et al*. 2000), *c*. 150–200 km from the trench.

It has been long thought that mantle melting in volcanic arc settings is triggered by fluxing of water and other volatiles, driven off the descending slab (Davies & Stevenson 1992; Stern 2002). The mechanism needed to focus volcanism into a narrow arc has been shown by Spiegelman & McKenzie (1987) to be an inevitable consequence of the geometry of the subduction zone. Any melt present will be driven by hydrodynamic pressure gradients into the corner, even if originating from dispersed regions at depth. The efficiency of this focusing depends on the viscosity of the corner flow, the porosity of the solid mantle, and the dip of the subducting slab. The remarkably world-wide consistency of the depth beneath the volcanic arc front to the top of the subducted slab suggests, however, that other factors such as the maximum depth at which significant slab dehydration occurs, and the position of the wet solidus isotherm in the overlying mantle wedge, are also likely to be important (Davies & Stevenson 1992; England *et al*. 2005).

Behind-arc magmatism tends to be much more variable in time and space and less voluminous compared with the steady-state arc volcanism, and is related perhaps to changes in the geometry of the subducted slab and overlying lithosphere (Coira

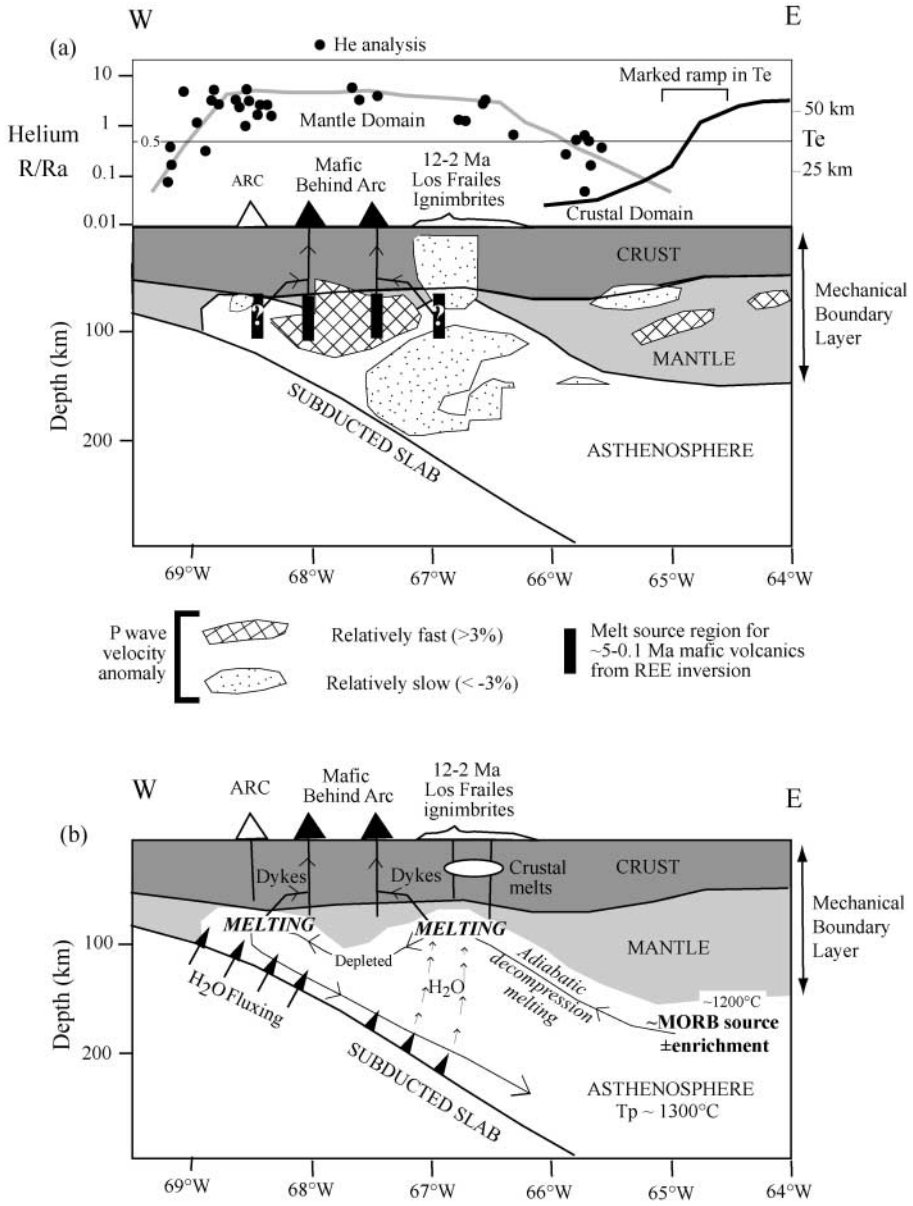

Fig. 11. Lithospheric scale cross-sections through the Central Andes in the vicinity of northern Chile and Bolivia, along 20°S, showing the location of the volcanic arc, as well as behind-arc mafic and ignimbritic volcanic activity. (**a**) Relative velocity anomalies for the P-wave tomographic model of Myers *et al*. (1998) are shown, as well as the melt source region determined from the REE inversions (see (**b**) for more detail). In addition, helium isotopic analyses (R/R_a values) for natural helium emissions are plotted along the profile, showing the extent of the mantle domain where helium derived from mantle degassing (mantle melting) dominates the helium emissions. It is clear that eastern and western limits of mantle helium degassing coincide with the edges of the P-wave 'slow' zones. However, a fast 'lid' beneath the Altiplano seems to occupy the melt zone of the Plio-Pleistocene mafic volcanic rocks. One possibility is that these volcanic rocks have been fed by lateral melt migration, in either the crust or the mantle, along dykes emanating from magma chambers beneath the volcanic arc and Los Frailes ignimbrites. The depth constraints on the melt zones, combined with tomographic and gravity studies, suggest that the mechanical boundary layer beneath the Andes thins from ⩾150 km in the east to ⩽100 km, farther west, beneath the western margin of the Eastern Cordillera, Altiplano and arc. (**b**) Cross-section based on (**a**), but showing possible mantle flow and melt conditions for a normal MORB-type source, with an asthenospheric potential temperature of *c*. 1300 °C. Melt generation beneath the Los Frailes region may be a consequence of upwelling in the corner flow, giving rise to adiabatic decompression melting under hydrous conditions (with only a very small water content). The depleted flow may continue on towards the arc, where further melting takes place as the flow experiences an intense water flux from the subducted slab. Enrichment of the melt zones may come from melting of the metasomatized thermal boundary layer.

et al. 1993; Kay & Abbruzzi 1996; Kay *et al*. 1999). However, Spiegelman & McKenzie (1987) showed that, even in a steady corner flow, hydrodynamic pressure gradients can both focus shallow melts and defocus melts from deeper source regions, so that they reach the surface over a wide region behind the arc. This defocusing will be greatest for high mantle porosities.

Plio-Pleistocene behind-arc volcanism

We use our REE inversions to understand the origin of the behind-arc Plio-Pleistocene volcanism in the Bolivian Andes. These suggest that the main melt source region from the western volcanic front and up to 150 km further east behind the arc is at relatively shallow depths <100 km (Figs 10 and 11). This source region is equated here with the thermal boundary layer, and is essentially a MORB-like source mantle modified by slab fluids and metasomatic melts. For the source region close to the arc itself, the inversion requires an initial *c*. 15% depletion of the MORB source, followed by a small enrichment from a MORB source and slab fluids. The mafic volcanic centres farther east, in a more distant behind-arc setting, require a melting model with an initial enrichment.

These geochemical constraints, taken together with the need to maintain arc volcanism over tens of millions of years, and both the fluid dynamical necessity of corner flow and the geometry of the Andean lithosphere, seem to be most easily explained by asthenospheric flow in MORB-source mantle that involves both upwelling and downwelling (Fig. 11b). The upwelling is an

inevitable consequence of the thinning of the Andean lithosphere towards the west, so that MORB-source asthenospheric mantle, as it is dragged towards the subduction corner, also flows upwards towards the base of the thinner lithosphere from a depth of *c*. 150 km beneath the Brazilian Shield to *c*. 65–75 km beneath the Central Andes. As long as a small amount of water is present, perhaps only 0.1%, then the upwelling under adiabatic conditions at temperatures greater than *c*. 1000 °C can be expected to cause decompression melting, with the rising melt maintaining hydrous conditions (Gaetani & Grove 1998), with the largest melt fractions being generated at the highest part in the melt column (Figs 10a,b, and 11b). It is interesting, in this respect, that the essentially linear increase in melt fraction with decreasing depth, rising from zero to *c*. 20% over the depth range of *c*. 100 km to 65 km, looks almost exactly like that predicted for many small oceanic islands, such as Inaccessible Island (McKenzie & O'Nions 1998).

It can be expected that melts generated near the top of the corner flow upwelling in the eastern part of the behind-arc region will eventually pool, together with the mantle helium, and rise into the overlying crust (mechanical boundary layer), either erupting at the surface as the eastern Plio-Pleistocene mafic volcanic centres, or becoming trapped. This process is probably going on today. The trapped magmas could then be the heat source for crustal melting (Annen & Sparks 2002), giving rise to ignimbrite eruptions on the western margin of the Eastern Cordillera (see below). The small enrichment required in the source region may come from either interaction with the metasomatized thermal boundary layer (McKenzie 1989) or an existing enrichment in the asthenosphere related to a much earlier episode of lithospheric entrainment (McKenzie & O'Nions 1995). The melt residue in the source region, now depleted, will still remain part of the overall corner flow, continuing its westward journey towards the volcanic arc (Figs 11b and 12d). If the lithosphere really does thicken slightly beneath the Altiplano, the flow may be slightly deflected downwards in this region, perhaps with some melt freezing, before rising again beneath the thin lithosphere in the arc region. Here, the flow may be fluxed by fluids driven off the subducting slab, triggering further melting that feeds the main arc volcanism, and perhaps also the Western Group of behind-arc volcanism. Again, enrichment could come from interaction with the metasomatized lithosphere and fluids coming off the slab. However, the source region is already depleted by the melt extraction farther east, providing a simple explanation for the initial depletion required by the REE abundances in the arc and Western Group of mafic behind-arc volcanic rocks.

Our model is similar to that of Woodhead *et al*. (1993) and Davidson (1996) to explain the depletion of non-fluid-mobile elements in island arcs associated with back-arc basins. The only difference is that, in the Andes, behind-arc melting is a consequence of upwelling where the thickness of the lithosphere decreases markedly towards the arc, rather than upwelling beneath a mid-ocean ridge in an extensional back-arc basin. In either case, the interaction between the corner flow and the overlying lithosphere exerts a profound influence on the generation of arc and behind-arc magmatism.

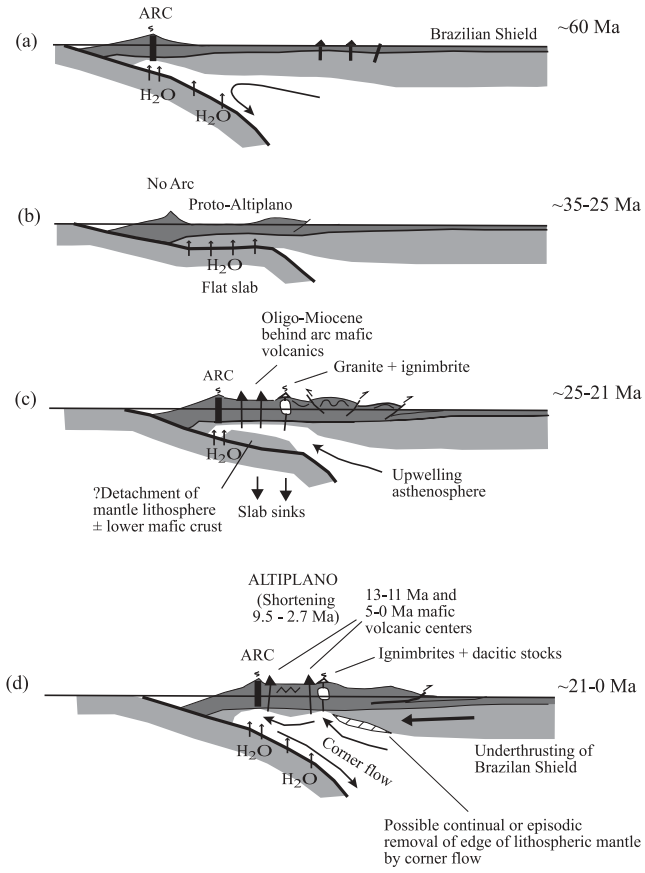

Fig. 12. Sketches illustrating the inferred lithospheric evolution and subduction zone melt generation for the Central Andes at *c*. 20°S. (**a**) In the Palaeocene (*c*. 60 Ma), volcanic activity was mainly confined to the arc, with a broad region behind (east of) the arc, >400 km wide, of subsidence. Deformation and uplift in the behind-arc region commenced at *c*. 40 Ma. (**b**) Between *c*. 35 and 25 Ma, arc volcanism shut off, which, by analogy with the present-day gap in the volcanic arc farther south, was probably caused by the squeezing out of the underlying asthenospheric wedge as a result of shallowing and flattening of the subducted slab. Water released from the flat slab would have hydrated the overlying mantle part of the lithosphere, weakening it. (**c**) Significant Andean lithospheric shortening in the Eastern Cordillera and Altiplano ceased at *c*. 30 Ma. However, arc volcanism, together with widespread behind-arc mafic–felsic volcanism, resumed abruptly at *c*. 25 Ma. The behind-arc mafic volcanism was the result of shallow mantle melting, most plausibly triggered by upwelling of hot asthenosphere into the newly formed wedge space caused by steepening of the subducted slab and detachment of part of the overlying weakened mantle lithosphere with possibly some of the mafic lower crust. This resulted in a thin lithosphere beneath the high Andes, which subsequently has remained largely unchanged. (**d**) The lithospheric structure, largely as it is today, with behind-arc and arc volcanism triggered by upwelling and hydrous fluxing in a corner flow. As thicker lithospheric mantle beneath the Eastern Cordillera is underthrust westward, it may be continually or episodically removed as it comes closer to the asthenospheric corner flow; episodic removal could trigger local uplift of the overlying crust.

Oligo-Miocene behind-arc volcanism

The Oligo-Miocene behind-arc mafic magmatic rocks potentially provide a powerful constraint on the earlier lithospheric structure. Their regional extent, with the development of sills and lava flows tens of metres thick, suggests melting over a wide region during a relatively restricted period of a few million years, between *c*. 25 Ma and *c*. 21 Ma, contemporaneous with the resumption of the main arc volcanism at *c*. 25 Ma, after a gap of *c*. 10 Ma when volcanic activity at the latitudes of Bolivia seems to have shut down (Fig. 11; James & Sacks 1999; Wörner *et al*. 2000). Building on the model of James & Sacks (1999), we

suggest that the 25–21 Ma behind-arc mafic event is related to the renewal of activity in the volcanic arc.

One possibility is that the magmatism in the Bolivian Andes is related to the change from flat slab subduction during the Oligocene (with its volcanic quiescence) to normal subduction, with the onset of magmatism right across the high part of the Bolivian Andes. Flat slab subduction has occurred since the mid-Miocene beneath northern Argentina and is still active at *c*. 30–32°S (Coira *et al*. 1993; Kay & Abbruzzi 1996; James & Sacks 1999; Kay *et al*. 1999), associated with marked gaps in the volcanic arc. James & Sacks (1999) pointed out that dehydration of the slab during flat subduction would hydrate, cool and weaken the overlying lithosphere over a wide area (Fig. 12b; James & Sacks 1999). In addition, a flat slab geometry in the Oligocene would have shifted the overlying asthenospheric wedge much farther east (Fig. 12b). If the tip of this wedge underlay the western margin of the Eastern Cordillera, then this would mark the eastern limit of lithospheric hydration and weakening (Fig. 12b).

If, just prior to *c*. 25 Ma, the slab began to steepen again, then this would have opened up a new wedge, possibly accompanied by the detachment of part of the overlying weakened lithospheric mantle with even part of the mafic lower crust, creating space into which adjacent asthenosphere could flow up and melt, as well as bringing enough heat to melt the remaining hydrated lithospheric mantle in a wide region behind the arc. In addition, this would result in a lithospheric structure with a mechanical boundary layer at depths <100 km (Fig. 12c). The detached part of the mantle lithosphere would be rapidly removed by the subduction process itself. If this did indeed include part of the mafic lower crust, then this would provide a simple explanation for the dominantly felsic composition of the crust beneath the Altiplano today (Beck & Zandt 2002). Seismic velocities for thickened lower continental crust suggest that at depths of *c*. 50 km, the bottom 10–20 km or so typically has a mafic garnet granulite composition with a density) (ρ) *c*. 3.1 g cm^{-3} (Christiansen & Mooney 1995). In this case, detachment of *c*. 15 km of mafic garnet granulite together with 50–100 km thickness of underlying mantle lithosphere (with a density of *c*. 3.3 g cm^{-3} and density contrast between asthenospheric and lithospheric mantle of *c*. −0.06 g cm^{-3}) would trigger <1 km of surface uplift in the overlying lithosphere. In other words, lithospheric delamination in this case would be associated with only a moderate surface uplift event.

OIB-like basalts erupting across the Altiplano are probably sourced from the inflowing asthenospheric mantle enriched by hydrated lithospheric mantle. (Figs 11b and 12). Once this mantle source had been exhausted, within a few million years, the extensive eruption of OIB-like basalts would cease, and normal arc activity, with a fully established corner flow, could continue. Mantle melts generated in this way are probably the heat source for anatectic wet melting of mid-crustal rocks. Thus, the granite plutons emplaced at *c*. 24 Ma on the western margin of the Eastern Cordillera, in the Cordillera Real, must represent the deeper crustal levels of this melting, whereas the arc and behind-arc dacitic to rhyodacitic lavas and stocks, as well as widespread ignimbrites, are the shallow-level and surface expression. The fact that this magmatic activity has been more or less continuous from *c*. 25 Ma to the present day strongly suggests that mantle melts have also been continuously introduced into the crust over this period, and the geothermal mantle helium emissions are the most recent expression of this (Fig. 8). It seems that only occasionally do the mantle melts actually reach the surface.

Discussion

We have used the geochemistry of behind-arc mafic magmatism and helium isotopes measured in natural gas emissions in geothermal and mineral-water springs to map out both the horizontal extent and depth of mantle melting beneath the Bolivian Andes. From this we infer both the present-day and *c*. 25 Ma lithospheric structure in this region. Our results suggest that a thin lithosphere, <100 km thick, existed beneath the high Andes in the Early Miocene and during the Plio-Pleistocene. However, we need to consider the lithospheric evolution in the intervening *c*. 15 Ma.

Significant crustal shortening in the Altiplano and Eastern Cordillera occurred mainly between *c*. 40 and 30 Ma (Lamb & Hoke 1997; Lamb *et al*. 1997; McQuarrie 2002). Subsequently, there was an intense phase of shortening in the central part of the northern Bolivian Altiplano between *c*. 9.5 Ma and 2.7 Ma (Lamb & Hoke 1997). In addition, the main phase of tectonic shortening farther east (mainly in the Sub-Andean zone) is younger than *c*. 10 Ma. This timetable of deformation suggests that between *c*. 25 Ma and *c*. 10 Ma we should not anticipate either significant lithospheric shortening, or concomitant thickening of the mantle lithosphere beneath the Altiplano greater than a few tens of kilometres, and thus the lithosphere here is likely to have remained thin over this period. However, Garzione *et al*. (2006) have suggested that there was a major phase of Late Miocene lithospheric thinning beneath the Bolivian Altiplano (implying unusually thick lithosphere just prior to this) to explain new estimates of the uplift history of the northern Bolivian Altiplano based on oxygen isotope measurements on carbonates, which suggest 2.5–3.5 km of rock uplift between *c*. 10 and 6.8 Ma, and essentially no uplift thereafter. This amount of uplift, if solely the result of mantle processes, would require rapid removal of a thickness of 140–580 km of lithospheric mantle, for a density contrast between lithospheric and asthenospheric mantle in the range 0.02–0.06 g cm^{-3} (Pulford & Stern 2004; Sobolev *et al*. 2006). It could also be explained by delamination of 35–80 km of pure mafic eclogite crust (3.45–3.55 g cm^{-3}), or some combination of mafic eclogite and mantle (Garzione *et al*. 2006; Sobolev *et al*. 2006).

It is clear that the uplift mechanisms proposed by Garzione *et al*. (2006) do not fit easily with the geological evolution of the Bolivian Andes determined in this study, constrained by the magmatic evidence, such as episodes of mafic volcanism at *c*. 25–21 Ma, *c*. 13–11 Ma, and 5–0 Ma, and more or less continuous widespread behind-arc intermediate–felsic magmatism since *c*. 25 Ma (Fig. 8). In addition, it seems implausible to us that the crust beneath the Altiplano at *c*. 10 Ma was >40% pure mafic eclogite and >100 km thick, with the subsequent detachment of a ≫40 km thick basal layer of the eclogite by 6.8 Ma. Certainly, such a thick eclogite layer could not be the result of Cenozoic (or Mesozoic) mafic magmatism behind the arc, as melt thicknesses at depth would not be expected to be more than a few kilometres, given the volume of surface eruptions (McKenzie 1984; Lamb & Hoke 1997). Also, the subducted slab beneath the volcanic arc is at a depth <120 km, and so unless the arc melt source in the Miocene was significantly deeper than that for volcanic arcs today, there is little room for thick Miocene mantle lithosphere here as well.

None the less, the westward underthrusting of thick lithosphere beneath the Eastern Cordillera might be expected to result in a westward migration of the edge of the zone of thin lithosphere (Fig. 12d). However, the position of the eastern limit of Neogene magmatism (Figs 1, 8, 11 and 12d) suggests that this has not

happened by more than 50 km, and much less than the 120–150 km of shortening in the Eastern Cordillera and Sub-Andean zone in the same period. This suggests that up to 100 km of westward underthrusting of mantle lithosphere has either been subducted beneath the western margin of the Eastern Cordillera deeper into the asthenospheric mantle (Sobolev *et al*. 2006) or has been counteracted by some form of lithospheric removal (Fig. 11). Continual removal will have no effect on surface uplift, because the lithospheric structure will remain constant, albeit with a marked step downwards to the east, where it thickens (Figs 11 and 12d). However, episodic removal on its own will give rise to uplift events. Thus, the catastrophic removal of the maximum possible 'excess' underthrust mantle would require detachment of a portion of mantle lithosphere *c*. 100 km long and up to 100 km thick (for a maximum lithospheric thickness beneath the Eastern Cordillera of *c*. 150 km). As a mechanism for Late Cenozoic uplift of the Altiplano, across a region *c*. 300 km wide, as suggested by Garzione *et al*. (2006), this clearly cannot account for regional uplift greater than 1 km, even if this includes removal of *c*. 15 km thickness of eclogitic lower crust. In addition, because the high heat flow in the Altiplano and western margin strongly suggests that these regions have a very low elastic thickness, uplift would be expected to be focused in the Eastern Cordillera and not the Altiplano. Finally, Barke & Lamb (2006) have shown that the distribution of observed Late Cenozoic crustal shortening in the Bolivian Andes can account for *c*. 2 km of uplift across the region since *c*. 10 Ma.

We conclude that the main features of the lithospheric structure beneath the Bolivian Altiplano had been established by *c*. 25 Ma. Even the felsic nature of the crust here can be attributed to detachment of the mafic lower crust (mafic garnet granulite) at this time. The establishment of upwelling in a mantle corner flow beneath this thin lithosphere since *c*. 25 Ma has allowed diffuse and long-lived adiabatic wet mantle melting to occur beneath the high Bolivian Andes. Some of these melts have reached the surface, but most have probably become lodged in the crust, providing the heat source for a protracted Miocene and younger history of crustal melting and granitic to intermediate intrusions that, today, are the host for much of Bolivia's mineral wealth. However, the Late Cenozoic evolution of this region appears to be different from that of the Altiplano of northern Argenina and southern Peru, where Kay & Kay (1993) and Whitman *et al*. (1996) have argued from both seismic attenuation and geochemical data that there has been significant delamination of the lithospheric mantle in the last 2 Ma, so that these regions are *c*. 1 km higher than the central and northern Altiplano in Bolivia (Whitman *et al*. 1996).

Conclusions

This paper describes the regional and temporal distribution of behind-arc mafic magmatism exposed in Bolivia, and the isotopic signature of natural helium emissions in geothermal and mineral-water springs in northern Chile, Bolivia and northern Argentina. The following conclusions can be drawn from these studies.

(1) There has been widespread mantle melting beneath the Bolivian Altiplano and western margin of the Eastern Cordillera in the Bolivian Andes since *c*. 25 Ma. The geochemistry of scattered mafic volcanic centres with ages of $\leqslant$5.3 Ma (and mainly $<$3.5 Ma), emplaced up to 150 km behind (east of) the volcanic arc, and regional Oligo-Miocene mafic eruptions and shallow intrusions with ages between *c*. 25 and 21 Ma, constrain the lithospheric evolution of the high Bolivian Andes.

(2) The isotopic signature of helium emissions in geothermal and mineral-water springs has been used to detect helium released by mantle degassing, probably through mantle melting. This suggests that a mantle melt zone and mantle melt extraction extends at *c*. 20°S from a few tens of kilometres west of the volcanic arc, in northern Chile, to the centre of the Bolivian Eastern Cordillera, over 300 km behind the arc and where the subducted slab is at a depth *c*. 250 km. There seems to be a clear relationship between topography and helium isotopes between 19° and 21°S, with a strong mantle helium component in gas emissions at altitudes $>$3600 m, suggesting that this region is in a thermal state that allows helium degassing, most plausibly because mantle melts and mantle melt extraction occur at depth.

(3) The REE in the behind-arc mafic volcanic rocks have been used, applying the method of McKenzie & O'Nions (1991), to invert for both the depth range of the melt source region and the nature of the source region itself. This shows that Plio-Pleistocene mafic volcanic centres were mainly generated by melting of a MORB source at depths $<$100 km. The best-fitting source region for the Eastern Group, which crops out between 100 and 150 km behind the arc, is slightly enriched, and very similar to that of small oceanic islands. The Western Group of similar volcanic centres, which crops out up to 75 km behind the volcanic arc front, was generated by melting of a depleted (*c*. 15%) MORB source, that was subsequently slightly enriched; the base of the melt source region for the Western Group may be up to 20 km deeper than that for the Eastern Group, reaching a depth of *c*. 120 km. Melting is likely to be occurring under hydrous conditions, with a mantle solidus at *c*. 1000–1200 °C. The Oligo-Miocene mafic volcanic rocks have been generated under very similar conditions to those for the eastern Plio-Pleistocene group, although more of the melt zone is predicted to be in spinel peridotite, extending to shallower depths than for the Plio-Pleistocene volcanic rocks, as predicted from the Neogene history of crustal shortening and thickening.

(4) A comparison of our results with the available high-resolution seismic tomography of the Bolivian Andes suggests that the lithosphere is thin ($<$100 km) beneath the Altiplano, but thickens towards the east, beneath the central and eastern parts of the Eastern Cordillera, to *c*. 150 km. To reconcile the seismically fast *c*. 125 km lithospheric root postulated by tomographic models (Myers *et al*. 1998) for the central part of the Altiplano, active melting could be focused into the regions beneath the western margin of the Eastern Cordillera, beneath the Los Frailes ignimbrites, and beneath the western front of the volcanic arc, where lithospheric mantle may not be present at all. In this case, lateral dyking of mafic melts, extending for up to 75 km outwards from these regions, may be responsible for advecting mantle melts and helium into the centre of the Altiplano.

(5) Behind-arc mantle melting is likely to be a consequence of adiabatic decompression in the upwelling part of the corner flow in the mantle wedge, controlled by the geometry of the overlying lithosphere where it thins markedly from east to west. Corner flow may have advected a depleted source region, generated behind the arc, into the melt zone beneath the arc, accounting for the difference in REE abundances between arc and behind-arc mafic volcanic rocks.

(6) Oligo-Miocene behind-arc mafic volcanism may have been triggered by changes in the mantle structure beneath the Bolivian Andes at *c*. 25 Ma and asthenospheric mantle upwelling during rapid steepening of an original flat subducted slab and detachment and local melting of weakened hydrated mantle lithosphere and possibly mafic lower crust, leading to the rapid re-establishment of volcanism right across the Bolivian Altiplano. There is

no obvious magmatic evidence for a marked change in lithospheric structure since then, and it is likely that the main features of the lithospheric structure beneath the Bolivian Andes have existed for the last 25 Ma, with crustal thickening in the Altiplano region achieved by both internal crustal shortening and the transfer of the thin-skinned crustal shortening in the Sub-Andes to ductile deformation in lower crustal levels beneath the Altiplano.

This work was supported by research grants from the Austrian Academy of Sciences, British Petroleum, the European Union, the Natural Environment Research Council (NERC) and the Royal Society of London. The REE inversions were kindly carried out by D. McKenzie, at the Bullard Laboratories, Cambridge University, on a Sun workstation, using the 1999 version of his INVMEL program (McKenzie & O'Nions 1991). We thank M. Wilson, S. deSilva and S. Kay for helpful reviews of an earlier version of this manuscript, and F. Stuart and two anonymous reviewers for comments on a later version.

References

Albarède, F. 1983. Inversion of batch melting equations and the trace element pattern of the mantle. *Journal of Geophysical Research*, **88**, 10573–10583.

Allmendinger, R.W., Jordan, T.E., Kay, S.M. & Isacks, B.L. 1997. The evolution of the Altiplano–Puna Plateau of the Central Andes. *Annual Review of Earth and Planetary Sciences*, **25**, 139–174.

Annen, C. & Sparks, R.S.J. 2002. Effects of repetitive emplacment of basaltic intrusions on thermal evolution and melt generation in the crust. *Earth and Planetary Science Letters*, **203**, 937–955.

Baker, M.C.W. & Francis, P.W. 1978. Upper Cenozoic volcanism in the Central Andes—ages and volumes. *Earth and Planetary Science Letters*, **41**, 175–187.

Ballentine, C.J. & Burnard, P.G. 2002. Production, release and transport of noble gases in the continental crust. *Reviews in Mineralogy and Petrology*, **47**, 481–529.

Barke, R. 2004. *Late Cenozoic tectonic and topographic evolution of the Bolivian Andes*. DPhil thesis, University of Oxford.

Barke, R. & Lamb, S. 2006. Late Cenozoic uplift of the Eastern Cordillera, Bolivian Andes. *Earth and Planetary Science Letters*, **249**, 350–367.

Barreiro, B., Jones, C. & Lamb, S. 1998. *U//Pb dating of zircons from the Quimse Cruz plutons, Bolivia*. Unpublished NERC Isotope Geosciences Laboratory (NIGL) report, Keyworth, UK.

Beck, S.L. & Zandth, G. 2002. The nature of orogenic crust in central Andes. *Journal of Geophysical Research*, **107**, doi: 10.1029/2000JB006124.

Beck, S., Zandt, G., Myers, S., Wallace, T., Silver, P. & Drake, L. 1996. Crustal thickness variations in the Central Andes. *Geology*, **24**, 407–410.

Black, E. 2000. *Lithospheric flexure in the Bolivian Andes*. DPhil thesis, University of Oxford.

Cahill, T. & Isacks, B.L. 1992. Seismicity and shape of the subducted Nazca plate. *Journal of Geophysical Research*, **97**, 17503–17529.

Christiansen, N.I. & Mooney, W.D. 1995. Seismic velocity structure and composition of the continental crust: a global view. *Journal of Geophysical Research*, **100**, 9761–9788.

Coira, B., Kay, S.M. & Viramonte, J. 1993. Upper Cenozoic magmatic evolution of the Argentinian Puna—a model for changing subduction geometry. *International Geological Review*, **35**, 677–720.

Davidson, J.P. 1996. Deciphering mantle and crustal signatures in subduction zone magmatism. *In:* Bébout, G.E., Scholl, D.W., Kirby, S.H. & Platt, J.P. (eds) *Subduction Top to Bottom*. Geophysical Monograph, American Geophysical Union, **96**, 251–262.

Davidson, J.P. & de Silva, S.L. 1992. Volcanic rocks from the Bolivian Altiplano: insight into crustal structure, contamination, and magma genesis in the Central Andes. *Geology*, **20**, 1127–1130.

Davidson, J.P. & de Silva, S.L. 1995. Late Cenozoic magmatism of the Bolivian Altiplano. *Contributions to Mineralogy and Petrology*, **119**, 387–408.

Davies, J. & Stevenson, D. 1992. Physical model of source region of subduction zone volcanics. *Journal of Geophysical Research*, **97**, 2037–2070.

DeMets, C., Gordon, R.G., Argus, D.F. & Stein, S. 1994. Effect of recent revisions on to the geomagnetic reversal time scale on estimates of current plate motions. *Geophysical Research Letters*, **21**, 2191–2194.

Dodson, A. & Brandon, A.D. 1999. Radiogenic helium in xenoliths from Simcoe, Washington, USA: implications for metasomatic processes in the mantle wedge above subduction zones. *Chemical Geology*, **160**, 371–385.

England, P.C. & Houseman, G.A. 1989. Extension during continental convergence, with application to the Tibetan Plateau. *Journal of Geophysical Research*, **94**, 17561–17579.

England, P.C., Engdahl, R. & Thatcher, W. 2005. Systematic variation in the depths of slabs beneath arc volcanoes. *Geophysical Journal International*, **156**, 377–408.

Evernden, J.F., Kriz, S.J. & Cherroni, C. 1977. Potassium–argon ages of some Bolivian rocks. *Economic Geology*, **72**, 1042–1061.

Fukao, Y., Widiyantoro, S. & Obayashi, M. 2001. Stagnant slabs in the upper and lower mantle transition region. *Reviews of Geophysics*, **39**, 291–323.

Gaetani, G.A. & Grove, T.L. 1998. The influence of water on melting of mantle peridotite. *Contributions to Mineralogy and Petrology*, **131**, 323–346.

Garzione, C.N., Molnar, P., Libarkin, J.C. & MacFaden, B.J. 2006. Rapid late Miocene rise of Bolivian Altiplano: evidence for removal of mantle lithosphere. *Earth and Planetary Science Letters*, **241**, 543–556.

Giggenbach, W.F. & Poreda, R.J. 1993. Helium isotopic and geochemical composition of gases from volcanic–hydrothermal systems in the Philippines. *Geothermics*, **22**, 369–380.

Graham, D.G. 2002. Noble gas isotope geochemistry of mid-ocean ridge and ocean island basalts: characterization of mantle source reservoirs. *Reviews in Mineralogy and Geochemistry*, **47**, 247–317.

Grant, J.W., Halls, C., Avial Salinas, W. & Snelling, N.J. 1979. K–Ar ages of igneous rocks and mineralisation in part of the Bolivian tin belt. *Economic Geology*, **74**, 838–851.

Hawkesworth, C.J., Hergt, J.M., McDermott, F. & Ellam, R.M. 1991. Destructive margin magmatism and the contributions from the mantle wedge and subducted crust. *Australian Journal of Earth Sciences*, **38**, 577–594.

Henry, S.G. & Pollack, H.N. 1988. Terrestrial heat flow above the Andean subduction zone in Bolivia and Peru. *Journal of Geophysical Research*, **93**, 15153–15162.

Hilton, D.R., Hammerschmidt, K., Teufel, S. & Friedrichsen, H. 1993. Helium isotope characteristics of Andean fluids and lavas. *Earth and Planetary Science Letters*, **120**, 265–282.

Hilton, D.R., Gronvold, K., Sveinbjornsdottir, A.E. & Hammerschmidt, K. 1998. Helium isotope evidence for off-axis degassing of the Icelandic hotspot. *Chemical Geology*, **149**, 173–187.

Hofmann, A.W. & Feigenson, M.D. 1983. Case study on the origin of basalt I. Theory and reassessment of Grenada basalts. *Contributions to Mineralogy and Petrology*, **84**, 382–389.

Hoke, L., Lamb, S.H. & Entenmann, J. 1993. Volcanic rocks from the Bolivian Altiplano: insight into crustal structure, contamination, and magma genesis: Comment and Reply. *Geology*, 1147–1149.

Hoke, L., Hilton, D.R., Lamb, S.H., Hammerschmidt, K. & Friedrichsen, H. 1994. ^{3}He evidence for a wide zone of active mantle melting beneath the Central Andes. *Earth and Planetary Science Letters*, **128**, 341–355.

Hoke, L., Lamb, S., Hilton, D. & Poreda, R. 2000. Southern limit of mantle-derived geothermal helium emissions in Tibet: implications for lithospheric structure. *Earth and Planetary Science Letters*, **180**, 297–308.

Houseman, G.A., McKenzie, D.P. & Molner, P. 1981. Convective instability of a thickened boundary layer and its relevance for the thermal evolution of continental convergent belts. *Journal of Geophysical Research*, **86**, 6115–6132.

James, D.E. & Sacks, I.W. 1999. Cenozoic formation of the Central Andes. a geophysical perspective. *In:* Skinner, B. (ed.) *Geology and Ore Deposits of the Central Andes*. Society of Economic Geologists, Special Publications, **7**, 1–25.

Kay, S. & Abbruzzi, J.M. 1996. Magmatic evidence for Neogene lithospheric evolution of the Central Andean 'flat-slab' between 30°S and 32°S. *Tectonophysics*, **259**, 15–28.

Kay, R.W. & Gast, P.W. 1973. The rare-earth content and origin of alkali-rich basalts. *Journal of Geology*, **81**, 653–682.

Kay, R.W. & Kay, S.M. 1993. Delamination and delamination magmatism. *Tectonophysics*, **219**, 177–189.

Kay, S., Coira, B. & Viramonte, J. 1994. Young mafic back arc volcanics as indicators of continental lithospheric delamination beneath the Argentine Puna plateau, central Andes. *Journal of Geophysical Research*, **99**, 24323–24339.

Kay, S.M., Mpodozis, C. & Coira, B. 1999. Magmatism, tectonism, and mineral deposits in the central Andes (22°–33°S). *In:* Skinner, B. (ed.) *Geology and Ore Deposits of the Central Andes*. Society of Economic Geologists, Special Publications, **7**, 27–59.

Kennan, L., Lamb, S.H. & Rundle, C. 1995. K–Ar dates from the Altiplano and Cordillera Oriental of Bolivia: implications for the Cenozoic stratigraphy and tectonics. *Journal of South American Earth Sciences*, **8**, 163–186.

Klein, E.M. & Langmuir, C.H. 1987. Global correlations of ocean ridge basalt chemistry with axial depth and crustal thickness. *Journal of Geophysical Research*, **92**, 8089–8115.

Lamb, S.H. 2000. Active deformation in the Bolivian Andes. *South America. Journal of Geophysical Research*, **105**, 25627–25653.

Lamb, S.H. & Hoke, L. 1997. Origin of the high plateau in the central Andes, Bolivia, South America. *Tectonics*, **16**, 623–649.

Lamb, S.H., Hoke, L., Kennan, L. & Dewey, J. 1997. Cenozoic evolution of the Central Andes in northern Chile and Bolivia. *In:* Burg, J.-P. & Ford, M. (eds) *Orogens Through Time*. Geological Society, London, Special Publications, **121**, 237–264.

Martelli, M., Nuccio, P.M., Stuart, F.M., Burgess, R., Ellam, R.M. & Italiano, F. 2004. Helium–strontium constraints on mantle evolution beneath the Roman Comagmatic Province, Italy. *Earth and Planetary Science Letters*, **224**, 295–308.

McKenzie, D. 1984. The generation and compaction of partially molten rock. *Journal of Petrology*, **25**, 713–765.

McKenzie, D. 1989. Some remarks on the movement of small melt fractions in the mantle. *Earth and Planetary Science Letters*, **95**, 53–72.

McKenzie, D. & Bickle, M.J. 1988. The volume and composition of melt generated by extension of the lithosphere. *Journal of Petrology*, **29**, 625–679.

McKenzie, D. & O'Nions, R.K. 1991. Partial melt distributions from inversion of rare element concentrations. *Journal of Petrology*, **32**, 1021-1091. (Corrections: *Journal of Petrology*, **33**, 1453 (1992).

McKenzie, D. & O'Nions, R.K. 1995. The source regions of ocean island basalts. *Journal of Petrology*, **36**, 133–159.

McKenzie, D. & O'Nions, R.K. 1998. Melt production beneath oceanic islands. *Physics of the Earth and Planetary Interiors*, **107**, 143–182.

McQuarrie, N. 2002. The kinematic history of the central Andean fold–thrust belt, Bolivia: implications for building a high plateau. *Geological Society of America Bulletin*, **114**, 950–963.

Minster, J.F. & Allègre, C.J. 1978. Systematic use of trace elements in igneous processes. Part III: inverse problem of batch partial melting in volcanic suites. *Contributions to Mineralogy and Petrology*, **69**, 37–52.

Molnar, P., England, P. & Martinod, J. 1993. Mantle dynamics, uplift of the Tibetan Plateau, and the Indian monsoon. *Reviews of Geophysics*, **31**, 357–396.

Myers, S.C., Beck, S., Zandt, G. & Wallace, T. 1998. Lithospheric-scale structure across the Bolivian Andes from tomographic images of velocity and attenuation for P and S waves. *Journal of Geophysical Research*, **103**, 21233–21252.

Ozima, M. & Podosek, F.A. 2002. *Noble Gas Geochemistry*. Cambridge University Press, Cambridge.

Pardo-Casas, F. & Molnar, P. 1987. Relative motion of the Nazca (Farallon) and South American plates since Late Cretaceous time. *Tectonics*, **6**, 233–248.

Pearce, J.A. 1983. The role of subcontinental lithosphere in magma genesis at distructive plate margins. *In:* Hawkesworth, C.J. & Norry, M.J. (eds) *Continental Basalts and Mantle Xenoliths*. Shiva, Nantwich, 230–249.

Pearce, J.A. & Parkinson, I.J. 1993. Trace element models for mantle melting: application to volcanic arc petrogenesis. *In:* Richard, H.M., Alabaster, T., Harris, N.B.W. & Neary, C.R. (eds) *Magmatic Processes and Plate Tectonics*. Geological Society, London, Special Publications, **76**, 373–403.

Platt, J.P. & England, P. 1994. Convective removal of the lithosphere beneath mountain belts: thermal and mechanical consequences. *American Journal of Science*, **294**, 307–336.

Pollack, H.N. & Chapman, D.S. 1977. On the regional variation of heat flow, geotherms, and lithospheric thickness. *Tectonophysics*, **38**, 270–296.

Poreda, R.J. & Farley, K.A. 1992. Rare gases in Samoan xenoliths. *Earth and Planetary Science Letters*, **113**, 129–144.

Pulford, A. & Stern, T. 2004. Pliocene exhumation and landscape evolution of central North Island, New Zealand: the role of the upper mantle. *Journal of Geophysical Research*, **109**, F01016, doi:10.1029/2003JF000046.

Ranalli, G. 1995. *Rheology of the Earth*, *2nd*. Chapman & Hall, London.

Redwood, S.D. & MacIntyre, R.M. 1989. K–Ar dating of Miocene magmatism and related epithermal mineralization of the northeastern Altiplano of Bolivia. *Economic Geology*, **84**, 618–630.

Schneider, A. 1985. *Eruptive processes, mineralization and isotopic evolution of the Los Friales–Kar Kari region, Bolivia*. DIC thesis, Imperial College, London.

Sempere, T., Herail, G., Oller, J. & Bonhomme, M. 1990. Late Oligocene–early Miocene major tectonic crisis and related basins in Bolivia. *Geology*, **18**, 496–949.

Sobolev, S., Babeyko, A., Koulakov, I. & Oncken, O. 2006. Mechanism of the Andean Orogeny: insight from numerical modeling. *In:* Oncken, O., Chong, G., Franz, G., *et al.* (eds) *The Andes, Active Subduction Orogeny*. Frontiers in Earth Sciences, 513–535.

Spiegelman, M. & McKenzie, D. 1987. Simple 2-D models for melt extraction at mid-ocean ridges and island arcs. *Earth and Planetary Science Letters*, **83**, 137–152.

Springer, M. 1999. Interpretation of the heat-flow density in the Central Andes. *Tectonophysics*, **306**, 377–395.

Stern, R.J. 2002. Subduction Zones. *Reviews of Geophysics*, 40.

Stewart, J. & Watts, A.B. 1997. Gravity anomalies and spatial variations of flexural rigidity at mountain ranges. *Journal of Geophysical Research*, **102**, 5327–5352.

Stuart, F.M., Lass-Evans, S., Fitton, J.G. & Ellam, R.M. 2003. High $^{3}He/^{4}He$ ratios in picritic basalts from Baffin Island and the role of a mixed reservoir in mantle plumes. *Nature*, **424**, 57–59.

Tainton, K.M. & McKenzie, D. 1994. The generation of kimberlites, lamproites and their source rocks. *Journal of Petrology*, **35**, 787–817.

Taylor, S.R., Arculus, R., Perfit, M.R. & Johnson, R.W. 1981. Island arc basalts. *In: Basaltic Volcanism on the Terrestrial Planets*. Pergamon, New York, 193–213.

Thorpe, R.S., Francis, P.W. & O'Callaghan, L. 1984. Relative roles of source composition, fractional crystallization and crustal contamination in the petrogenesis of Andean rocks. *Philosophical Transactions of the Royal Society of London, Series A*, **310**, 675–692.

Turcotte, D.L. & Schubert, G. 2002. *Geodynamics*. Cambridge University Press, Cambridge.

Van der Hilst, R.D. & Karason, H. 1999. Compositional heterogeneity in the bottom 1000 kilometers of Earth's mantle: Toward a hybrid convection model. *Science*, **283**, 1885–1888.

Van der Lee, S., James, D. & Silver, P. 2001. Upper mantle S velocity structure of central and western South America. *Journal of Geophysical Research*, **106**, 30821–30834.

Watson, S. & McKenzie, D. 1991. Melt generation by plumes: a study of Hawaiian volcanism. *Journal of Petrology*, **32**, 501–537.

Watts, A.B., Lamb, S.H., Fairhead, J.D. & Dewey, F.J. 1995. Lithospheric flexure and bending of the Central Andes. *Earth and Planetary Science Letters*, **134**, 9–21.

Whitman, D., Isacks, B.L., Chatelain, J.L., Chiu, J.M. & Perez, A. 1992. Attenuation of high-frequency seismic waves beneath the Central Andean plateau. *Journal of Geophysical Research*, **97**, 19929–19947.

Whitman, D., Isacks, B.L. & Kay, S.M. 1996. Lithospheric structure and along-strike segmentation of the central Andean plateau: seismic q, magmatism, flexure, topography and tectonics. *Tectonophysics*, **259**, 29–40.

Widiyantoro, S. & van der Hilst, R.D. 1997. Mantle structure beneath Indonesia inferred from high-resolution tomographic imaging. *Geophysical Journal International*, **130**, 167–182.

Wigger, P., Schmitz, M. & Araneda, M. *et al.* 1993. Variation in the crustal structure of the southern central Andes deduced from seismic refraction investigations. *In:* Reutter, K.-J., Scheuber, E. & Wigger, P.*et al.* (eds) *Tectonics of the Southern Central Andes*. Springer, Berlin, 23–48.

Woodhead, J.D., Eggins, S.E. & Gamble, J.G. 1993. High field strength and transition element systematics in island arc and back-arc basin basalts: evidence for multiphase extraction and a depleted mantle wedge. *Earth and Planetary Science Letters*, **114**, 491–504.

Wörner, G., Harmon, R.S. & Davidson, J. *et al.* 1988. The Nevados de Payachata volcanic region (18°S/69°W, N. Chile). I. Geological, geochemical, and isotopc variations. *Bulletin of Vulcanology*, **50**, 287–303.

Wörner, G., Hammerschmidt, K., Henjes-Kunst, F., Lezaun, J. & Wilke, H. 2000. Geochronology ($^{40}Ar/^{39}Ar$, K–Ar and He-exposure ages) of Cenozoic magmatic rocks from Northern Chile (18–22°S): implications for magmatism and tectonic evolution of the central Andes. *Revista Geologica de Chile*, **27**, 205–240.

Yuan, X., Sobolev, S.V. & Kind, R. *et al.* 2002. Subduction and collision processes in the Central Andes constrained by converted seismic phases. *Nature*, **408**, 958–961.

Received 14 June 2006; revised typescript accepted 23 January 2007.
Scientific editing by Sally Gibson